2016

Synthesis of Porous Manganese Oxides with Unsaturated Alcohols and Subsequent Characterization and Catalytic Activity

Chrismary De La Cruz
Connecticut College

Synthesis of Porous Manganese Oxides with Unsaturated Alcohols and Subsequent Characterization and Catalytic Activity

Chrismary De La Cruz ‘16

Department of Chemistry, Connecticut College

New London, CT 06320

Advisor: Professor Stanton Ching

Table of Contents

Acknowledgments

First and foremost, I would like to start off by thanking professor Stanton Ching, more affectionately known as Stan, for giving me the wonderful opportunity of working in his research lab. Stan allowed me to join his research group the summer after my freshmen year and I was able to learn what it really meant to work in a lab. Stan gave me continuous guidance but also so much independence. Because of this I was able to grow as a scientists and learned how to think critically for myself. His famous smile and friendly attitude made my experience an extremely pleasant one and I was happy to return to work in his lab the next summer, after my sophomore year. I am most grateful however, for his approval to do an honors thesis. A slightly last minute request, there were doubts on whether I would actually be able to accomplish the huge feat that is an honors thesis as I only had two summers of experience in his lab, and previous thesis students had upwards of two years. However, Stan had faith in my abilities and allowed me to pursue the honors study. And now, one year later, I've successfully completed my thesis and I cannot thank him enough for believing in me. Stan truly is "the man" Ching.

Next, I would like to take Marc Zimmer for his continual support over my 4 years at Connecticut College. Marc truly is my "day 1," as he was the first professor I met once I arrived to Conn for the Science Leaders orientation. Marc was my advisor through the Science Leaders program, and through him, I was able to secure my summer internships at Conn. Not only did he put me in contact with many of the professors in the chemistry department, including Stan, but also constantly helped me to secure the funding for my

work. Together with Stan, I can genuinely say that Marc has been one of my biggest influences during my studies here at Connecticut College.

I would also like to thank Steve Suib, along with Marc, for reading my thesis and giving me valuable feedback.

Further I would like to thank Jeffrey Carmichael ’14 for teaching me all the basics the summer after my freshmen year and helping me get accustomed to the lab setting. Also, Ian Richter 14’ for all of his work on the butanol spheres, which gave the inspiration for my research. Finally, I want to give a huge thank you to Dezmond Bishop ’16 for his work on synthesis was unsaturated alcohols, as my thesis would not have been possible at all without his research and valuable input.

Lastly, I want to thank my best friends for their continuous support over the years, and especially during my honors thesis. So, a big thank you to Anthony Guerrero ’16, Sergio Madera ’16, Shelly Rodriguez ’16 and Eduardo Araujo ‘16.

Abstract

Porous manganese oxides have been synthesized using unsaturated alcohols (allyl alcohol and propargyl alcohol) as reducing agents in a redox reaction with $KMnO_4$ in the presence of butyric acid. Materials have an approximate MnO_2 stoichiometry and surface areas of 280 m^2/g for materials made with allyl alcohol and 260 m^2/g for those made with propargyl alcohol. Materials also showed a good deal of monodispersity, with the materials made from allyl alcohol having an average diameter of 156 nm± 61 nm. The materials made with propargyl alcohol had an average diameter of 143 nm ±49 nm.

Previously, highly monodisperse porous spheres were synthesized using butanol as the reducing agent in a redox reaction with $KMnO_4$ in the presence of butyric acid. It was hypothesized that since allyl alcohol and propargyl alcohol have a similar polarity to butanol, similar monodisperse, porous spheres would form. However, due to the presence of multiple reactive sites, materials made with the unsaturated alcohols would be formed quicker, have a smaller particle size, and have higher surface areas when compared to those made with butanol. This thesis reports on these findings and the confirmation of our hypothesis.

These materials have also proven to be active catalysts in the conversion of isopropyl alcohol to acetone. Conversions percentages were about 90% for the materials made with ally alcohol at 200°C and about 94% for materials made with either propargyl alcohol or allyl alcohol at 250°C.

Lastly, doping of these materials with metal cations followed by heat treatment, calcination or hydrothermal, led to formation of several crystalline structures such as spinel, birnessite, and cryptomelane, among others.

Introduction

Manganese oxides are a class of synthetic and naturally occurring materials that are commonly found in mineral forms that include soils, sediments and ores. They are also found in desert rock varnish and deep-sea nodular deposits.[1] Desert rock varnish forms as the result of decomposing bodies of microorganisms that utilize manganese ions biochemically and leave behind a film of manganese oxide, Figure 1. Historically, Native Americans took advantage of this varnish to create petroglyphs, images created by the carving of a rock's surface. Rock varnish can be found in dry desert areas throughout the southwestern United States.

Photo by Neal Herbert Photo by Joel Duff

Figure 1. From left to right: Desert varnish streaks and petroglyphs

Deep-sea nodules (Figure 2) form over the course of millions of years and are mainly made up of manganese oxides and iron oxides, though their exact composition varies based on their location.[2] The nodules form around a nucleation site, which can be anything from a grain of sand to a shark tooth. In addition to manganese and iron, the nodules have been found to contain several other transition metals in much higher

concentration compared to their oceanic abundance. Nodules have been shown to have a high percentage of Ni, Co, and Cu, among other metals, and so have become of interest as a potential source for these metals through nodule mining.[3]

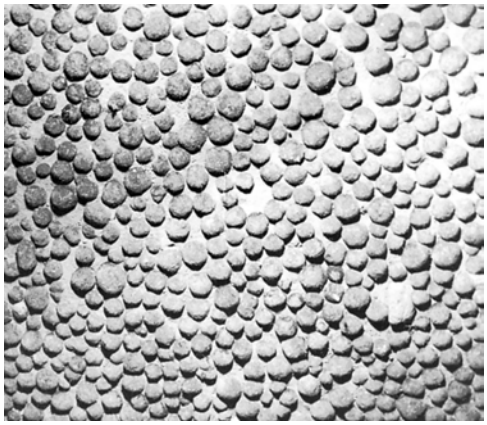

Photo by *Lamont-Doherty Geological Observatory*
Figure 2. Deep sea nodules on the Pacific Ocean floor

Despite relatively simple stoichiometry (MnO_2 or approximately MnO_2), manganese oxides are extremely diverse. They come in a wide array of structures, including layered and tunneled, porous and nonporous, as well as amorphous and crystalline. Structures commonly consist of edge-shared MnO_6 octahedra and it is not unusual to find interstitial cations and water molecules within their frameworks. Structures of some well-studied crystalline manganese oxides are shown below in Figure 3. Birnessite is composed of sheets of MnO_6 octahedra with cations and water molecules occupying the interstitial space. Pyrolusite, hollandite, and todorokite have tunneled structures with 1x1, 2x2, and 3x3 arrays of MnO_6 units, respectively, defining the tunnel size. Of these, pyrolusite is the only nonporous material, since the 1x1 tunnel is too small to accommodate ions or molecules. It also has precise MnO_2 formulation. Birnessite,

hollandite, and todorokite have microporous structures that contain cations and water molecules within the interlayer or tunnel sites. The presence of cations requires charge balance through Mn(III)/Mn (IV) mixed valency, which gives overall negative charge to the manganese oxide framework. The interstitial cations enables these materials to be used in cation exchange, while the mixed valency gives rise to semiconductive properties by electron hopping mechanism. [4-6]

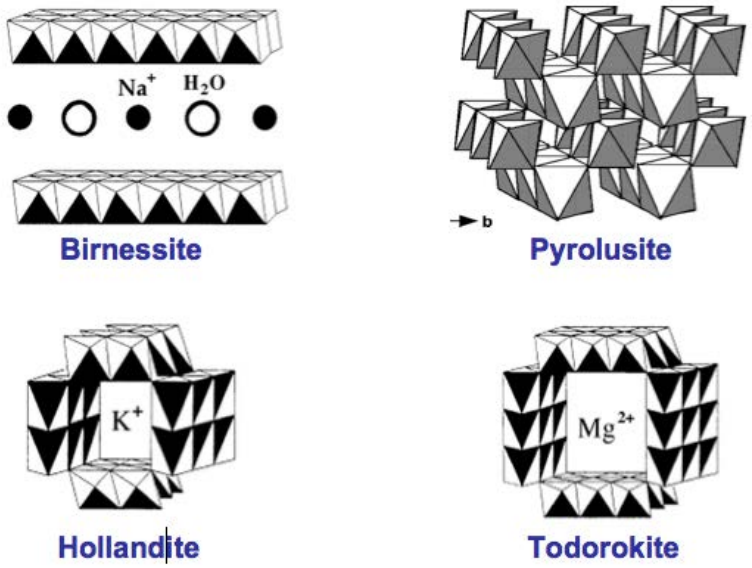

Figure 3. Different types of crystalline layered and tunnel manganese oxides

An extremely important property of these porous manganese oxides is their high surface area, which is made possible by the considerable amount of internal surface in the porous structure. High surface area materials are useful in a variety of major applications such as heterogeneous catalysis, hazardous waste remediation, and rechargeable battery technology.[7-9] Another desirable characteristic of manganese oxides are their low cost and low toxicity, both of which are highly beneficial to large-scale applications.

Heterogeneous catalysis has many potential uses in a variety of fields including petrochemsistry[10-11], food production[12-13] and the car manufacturing industry. [14-15] Manganese oxides have been shown to successfully catalyze oxidation reactions such as the conversion alcohols into carbonyl compounds[16-18], oxidation of carbon monoxide into carbon dioxide [19-21], and total combustion of hydrocarbons. These reactions are believed to follow the Mars Van Krevelin mechanism, in which Mn shuttles between its 4+ and 2+ oxidation states while framework oxygen is given up to oxidize organic substrates and then replenished by reduction of molecular O_2. The mechanism is outlined in Figure 4 for the oxidation of isopropanol to acetone.

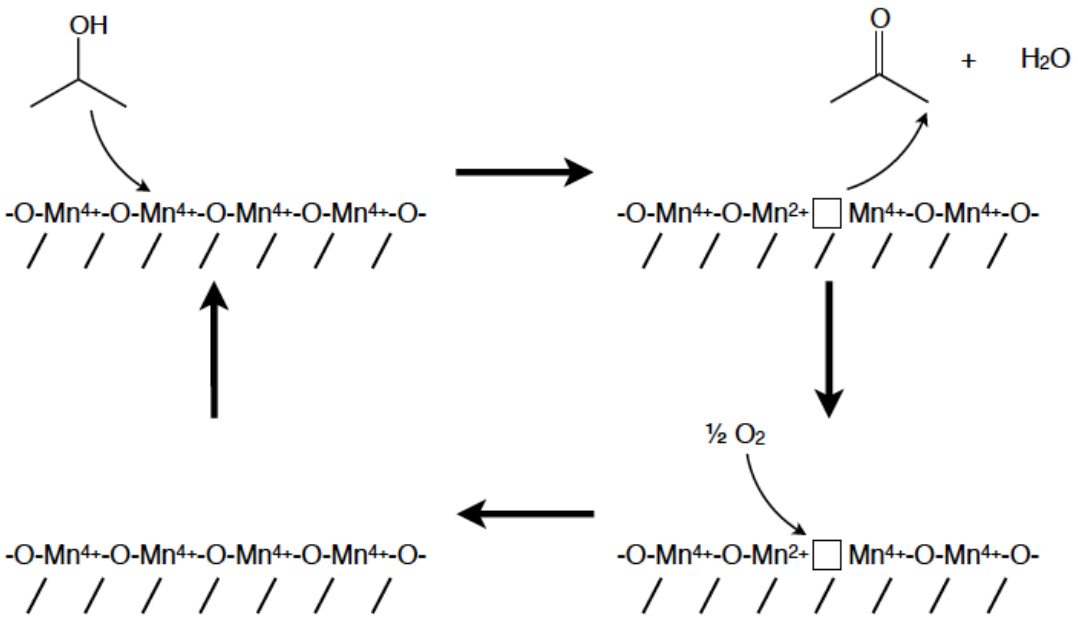

Figure 4. Mars Van Krevelin mechanism for manganese oxide catalysis of isopropyl alcohol to acetone

Many synthetic routes have been used to prepare porous manganese oxides. Some examples include aqueous precipitation [21,22] hydrothermal treatment [23,24] sol-gel processing [25,26], and high-temperature solid-state reactions.[27] Different methods and

reaction conditions are used to generate different morphologies for materials with the same manganese oxide structure. This, in turn, can influence particles size, surface area, and catalytic activity. Some observed morphologies include rod-like, flower-like[23], honeycomb[28], urchin, and cocoon-like structures. [29]

A hollow nanostructure morphology is also possible and can be achieved through a variety methods, including hydrothermal synthesis. In a hydrothermal process, a solution of Mn^{2+} and permanganate is placed in an autoclave and subjected to high temperature and pressure. This reaction is typically a lengthy one, lasting anywhere from a couple of hours to several days. [30] The formation of these hollow nanostructures proceeds through the process of Ostwald ripening, exemplified in Figure 5. Ostwald ripening is a phenomenon that occurs as the result of smaller, more soluble particles dissolving in solution and re-depositing on the surface of larger particles, creating a central cavity. Through this process, several types of hollow morphologies can be produced, including core shell and multi-shelled, Figure 6, as well an asymmetric hollowing of the nanostructures, Figure 7. [31]

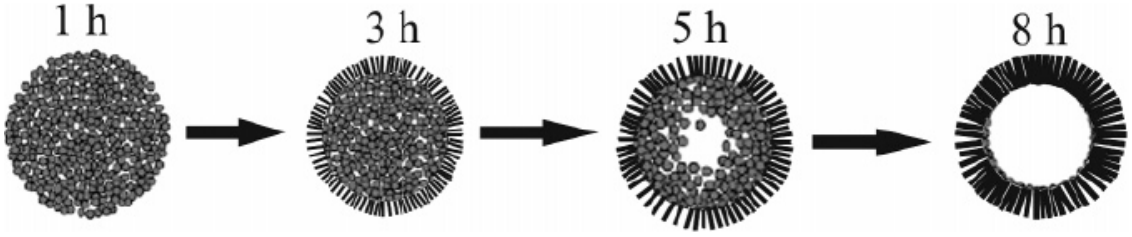

Figure 5. Ostwald Ripening phenomenon over the course of 8 hours. [31]

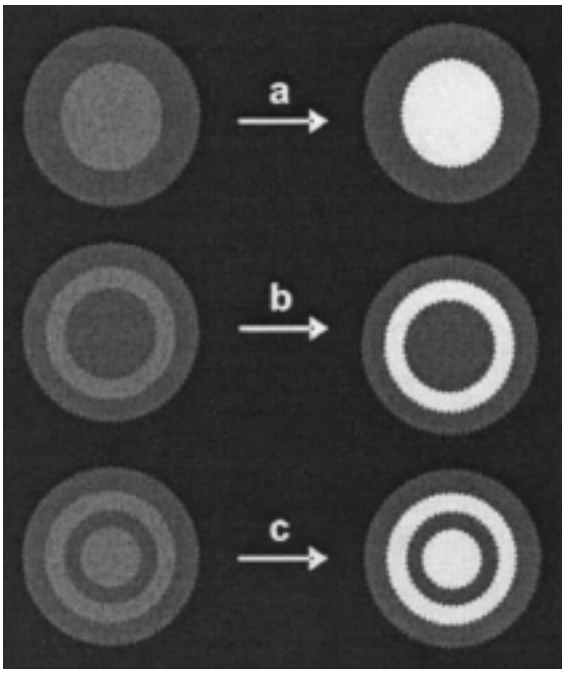

Figure 6. Ostwald ripening induced morphologies including a) basic central cavity b) core-shell and c) multi-shelled.[31]

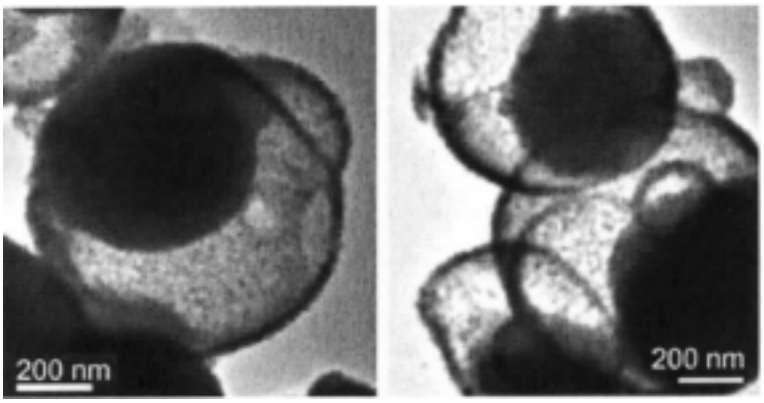

Figure 7. Asymmetric hollowing of nanospheres [31].

Recently, the Ching research group made significant contributions to the synthesis of porous manganese oxide materials by developing facile, one pot syntheses of hollow spherical and porous spherical manganese oxides with very high surface areas and excellent control over particle size and morphology. These were carried out through precipitation redox reactions using MnO_4^- as the oxidizing agent and either Mn^{2+} or butanol as the reducing agent, with butyric acid present as both a structure-directing

template and nanoparticle-inducing ligand. The inspiration for this research stems from a manganese molecular cluster, $Mn_{12}O_{12}(O_2CCH_3)_{16}(H_2O)_4$, which has a Mn_{12} core consisting of edge-shared MnO_6 octahedra analogous to what is observed in manganese oxide materials, Figure 8. The Mn_{12} cluster core is stabilized by acetate ligands and the molecule is prepared by reacting alkylammonium permanganate with Mn^{2+} in concentrated aqueous sodium acetate/acetic acid solution.[32] The goal of the Ching group was to combine molecular and materials syntheses in a "bottom up" strategy that promotes the expansion of the molecular cluster core into that of a material while capping particle size at nanoscale dimensions using carboxylic acid ligands to stymie particle growth. The result would be high surface area materials that are desirable in many of the potential applications of manganese oxides that require interfacial interactions, such as in catalysts, sorbents, and battery materials. The "bottom up" strategy is in contrast to a "top down" approach, Figure 9, of physical grinding of larger particles, which is unable to achieve nano scale particle dimensions.

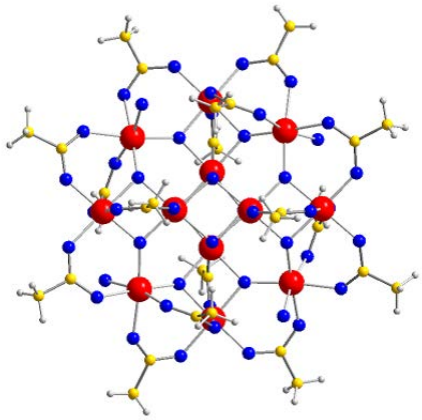

Figure 8. $Mn_{12}O_{12}(O_2CCH_3)_{16}(H_2O)_4$. cluster stabilized by carboxylate ligands (yellow)[32]

Figure 9. “Top down” approach of grinding salt crystals

In the synthesis of manganese oxide spheres, MnO_4^- reacts with reducing agent Mn^{2+} in a common reaction conducted to synthesize porous manganese oxides. These spheres, shown in Figure 10, exhibit hierarchal structure. When observed at low magnifications, such as through the use of SEM, they seem to be solid spheres. However, under closer inspection with TEM, it is apparent that the spheres are composed of large sheets, aggregating together to form these nanospheres. This aggregation of sheets is coined the “crumpled tissue” morphology.

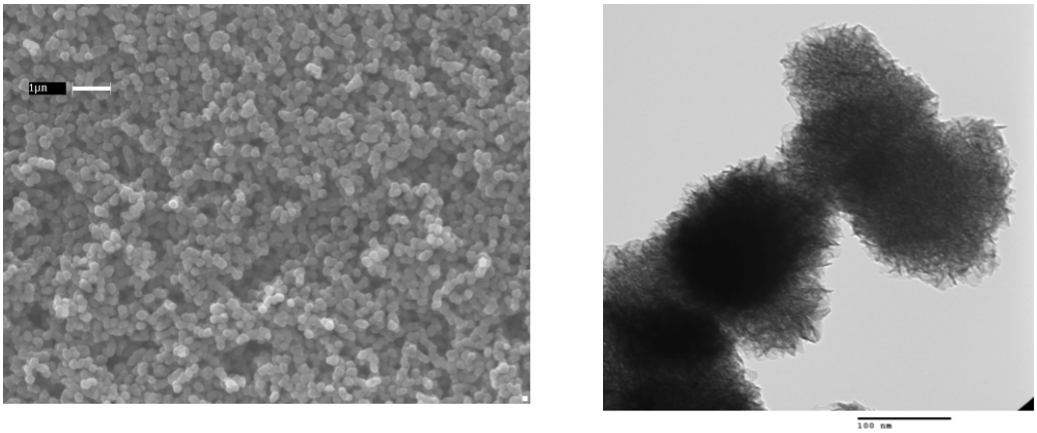

Figure 10. Control reaction with no carboxylic acid, left to right: SEM and TEM image highlighting hierarchal structure

To test our “bottom up” approach, this reaction was carried out in the presence of several carboxylic acids including acetic acid, propionic acid, and butyric acid. The latter resulted in the most interesting morphology of hollow spheres.[21] The mechanistic explanation for the formation of these hollow spheres is rooted in aqueous microemulsion

formed by butyric acid, which is not fully miscible in water. The presence of these microemulsions has been confirmed by observation of the Tyndall effect, Figure 11. These microemulsions act as a soft template on which nanoparticle manganese oxide can form. Both Mn^{2+} and $KMnO_4$ favor the aqueous phase and react in the aqueous phase, with the resulting nanoparticles forming and aggregating around the microemulsion template. When the material is finally washed, the template is removed and the resulting materials are hollow spheres, Figure 12. These spheres also exhibit a hierarchal structure, and are composed of tiny platelets aggregating together to produce the hollow spheres, Figure 13. While other methods can be used to form hollow spheres, including the previously mentioned Ostwald ripening under hydrothermal conditions, these other methods tend to be expensive, require harsh conditions, and can take several hours, or even days to complete. [21,22,30,31]

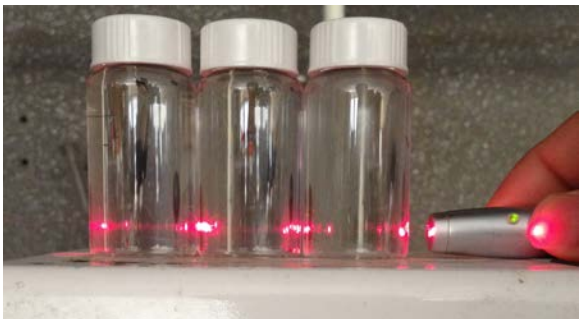

Fig 11. The Tyndall effect is shown above as light passes through (from left to right) solutions of butyric acid/water, butyric acid/MnSO4/water, and butyric acid/ butanol/water.

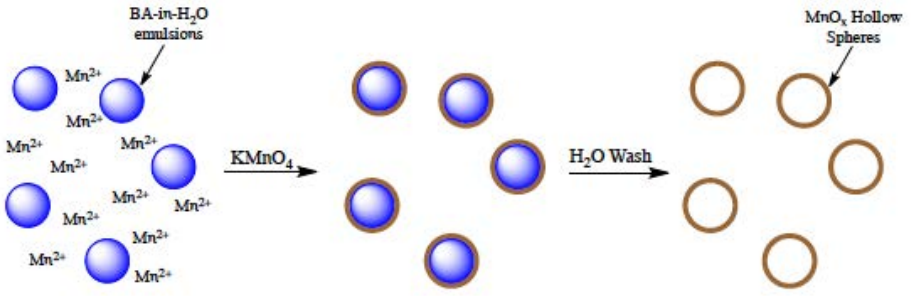

Figure 12. Proposed mechanism for the formation of the manganese oxide hollow spheres

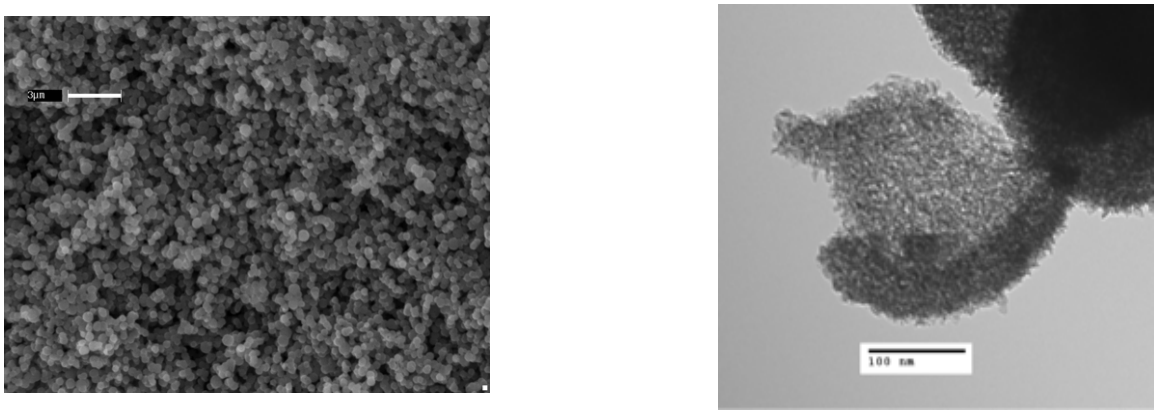

Figure 13. From left to right, MnOx formed in the presence of butyric acid: SEM image (1 uM scale bar) and TEM image

Manganese oxide nanoparticles can also be prepared as highly monodisperse porous spheres when butanol, in place of Mn^{2+}, is used as the reducing agent. [22] In this reaction, butanol is a more nonpolar molecule that prefers to be in the organic phase. Butanol in this case partitions into the butyric acid emulsion. Thus, for $KMnO_4$ to react with butanol, it must also enter the emulsion. The resulting nanoparticles will then form and aggregate inside the emulsion. Once the product is washed, the template is once again removed and the resulting material are porous spheres, Figure 14. The resulting material is extremely monodisperse and similar to the previous material mentioned, exhibits a hierarchal structure, Figure 15.

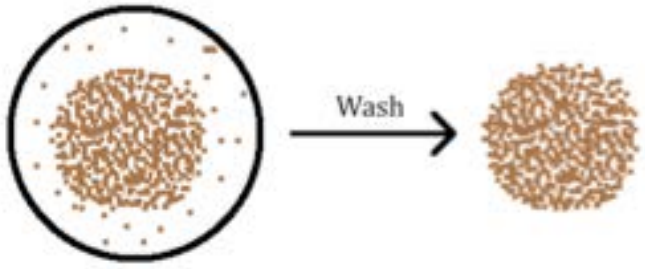

Figure 14. Proposed mechanism for the formation of porous spheres with butanol as the reducing agent

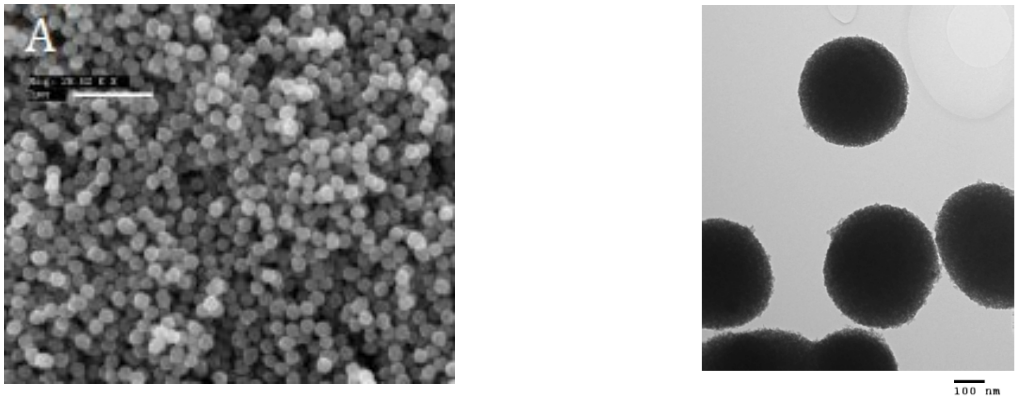

Figure 15. From left to right, MnOx formed in the presence of butyric acid, with butanol as the reducing agent: SEM image and TEM image

In this research, allyl alcohol and propargyl alcohol are used as reducing agents in reactions with permanganate in the presence of butyric acid. These reactions were pursued for two main reasons. Firstly, allyl alcohol and propargyl alcohol partition into the butyric acid emulsion in a similar fashion to that of butanol, and so likely proceed through the same mechanism. And secondly, there is the presence of multiple reactive sites on these molecules, with both double/triple bond and the alcohol group. This feature enhances the reactivity of the molecules and is hypothesized to lead to a faster reaction. A faster reaction in theory should lead to more nucleation sites, which in turn, would result in smaller particle sizes and higher surface area materials.

Experimental

Chemicals and General Procedures

Reagent-grade chemicals were obtained from VWR Scientific and used as received. Distilled water was used throughout. MnOx nanoparticles were calcined in a Lindberg/Blue M Tube Furnace. Hydrothermal reactions were carried out in 30 mL Teflon-lined autoclaves.

Synthesis

Manganese Oxide Porous Spheres from Allyl Alcohol

In a typical synthesis, 0.158 g (1.00 mmol) of $KMnO_4$ was dissolved in 25 mL water, which was added to a vigorously stirred solution containing 2.3 mL (25.0 mmol) of butyric acid and 0.068 mL (1.00 mmol) of allyl alcohol in 25 mL of water. The reaction mixture immediately turned reddish brown, followed by the formation of brown solid. After 20 minutes of stirring, the brown precipitate was collected by vacuum filtration through a medium porosity frit, washed three times with water, and allowed to dry at 110 °C. An isolated mass of 0.07 g was typical.

Porous Spheres with Propargyl Alcohol

Typical synthesis reactions were done with a ratio of 0.3:1 propargyl alcohol:Mn. A 0.158 g sample of $KMnO_4$ (1.00 mmol) was dissolved in 25 mL water. Separately, 2.3 mL of butyric acid (25 mmol) and 0.175 mL (3 mmol) of propargyl alcohol were added to 25 mL of water. The $KMnO_4$ solution was added to the butyric acid/alcohol solution and allowed to stir vigorously. The reaction mixture immediately turned reddish brown, followed by the formation of brown solid. After 20 minutes of stirring, the brown

precipitate was collected by vacuum filtration through a medium porosity frit, washed three times with water, and allowed to dry at 110 °C. An isolated mass of 0.039 g was typical.

Porous Spheres with Ethylene Glycol

In a typical synthesis, 0.158g of $KMnO_4$ (1 mmol) was dissolved in 25 mL water, which was added to a vigorously stirred solution containing 2.3 mL (25.0 mmol) of butyric acid and 0.056 mL (1 mmol) of ethylene glycol in 25 mL of water. The reaction was allowed to stir overnight, until a brown precipitate was seen. After, the brown precipitate was collected by vacuum filtration through a medium porosity frit, washed three times with water, and allowed to dry at 110 °C.

Porous Spheres with Glycerol

In a typical synthesis, 0.158g of $KMnO_4$ (1 mmol) was dissolved in 25 mL water, which was added to a vigorously stirred solution containing 2.3 mL (25.0 mmol) of butyric acid and 0.073 mL (1 mmol) of glycerol in 25 mL of water. The reaction was allowed to stir for 3 hours, until a brown precipitate was seen. After, the brown precipitate was collected by vacuum filtration through a medium porosity frit, washed three times with water, and allowed to dry at 110 °C.

Doping

Isomorphous Doping of MnOx Nanoparticle Spheres

Copper Doping

A 0.158 g sample of $KMnO_4$ (1 mmol) was dissolved in 25 mL water. Separately, 2.3 mL (25 mmol) of butyric acid, 0.068 mL (1 mmol) of allyl alcohol and 0.03993 g (0.2 mmol) of $Cu(OAc)_2$ x H_2O were dissolved in 25 mL of water. The $KMnO_4$ solution was mixed with alcohol solution and allowed to stir. The reaction mixture immediately turned reddish brown, followed by the formation of brown solid. After 20 minutes of stirring, the brown precipitate was collected by vacuum filtration through a medium porosity frit, washed three times with water, and allowed to dry at 110 °C. Similar reactions were done with 0.175 mL (3 mmol) of propargyl alcohol replacing the allyl alcohol.

Iron Doping

A 0.158 g (1 mmol) sample of $KMnO_4$ was dissolved in 25 mL water. Separately, 2.3 mL (25 mmol) of butyric acid, 0.068 mL (1 mmol) of allyl alcohol and 0.05861g (0.15 mmol) of $Fe(NH_4)_2(SO_4)_2$•$6H_20$ were dissolved in 25 mL of water.. The $KMnO_4$ solution was then added to the alcohol solution and allowed to stir. The reaction mixture immediately turned reddish brown, followed by the formation of brown solid. After 20 minutes of stirring, the brown precipitate was collected by vacuum filtration through a medium porosity frit, washed three times with water, and allowed to dry at 110 °C. Similar reactions were done with 0.175 mL (3 mmol) of propargyl alcohol replacing the allyl alcohol.

Cerium Doping

A 0.158 g (1 mmol) sample of of $KMnO_4$ was dissolved in 25 mL water.

Separately, 2.3 mL (25 mmol) of butyric acid, 0.068 mL (1 mmol) of allyl alcohol and 0.0689g (0.2 mmol) of $Ce(OAc)_3 \cdot 1.5\ H_2O$ were dissolved in 25 mL of water. The $KMnO_4$ solution was then added to the alcohol solution and allowed to stir. The reaction mixture immediately turned reddish brown, followed by the formation of brown solid. After 20 minutes of stirring, the brown precipitate was collected by vacuum filtration through a medium porosity frit, washed three times with water, and allowed to dry at 110 °C. Similar reactions were done with 0.175 mL (3 mmol) of propargyl alcohol replacing the allyl alcohol.

Insipient Wetness Doping with Alkali Metals

In a typical synthesis reaction, 0.12-0.15 g of previously synthesized MnOx with allyl alcohol was added to 10 mL of water and allowed to dissolve. Next, the alkali metal acetate (Na/ K/ Li) was added to the solution in either 0.25:1, 0.5:1, or 1:1 metal: Mn molar ratios. The mixture was allowed to stir for an hour and then dried in an oven at 110°C. Once the product was dried, it was calcined at 450°C for 2 hours. Separately, products doped with potassium were also calcined at 600°C for 2 hours.

Insipient Wetness Doping and Hydrothermal Treatment

In a typical synthesis, 0.06-0.12 g of previously synthesized MnOx from allyl alcohol was dissolved in 10 mL of distilled water. Magnesium sulfate was added in a 1:1 Mn:Mg molar ratio. The solution was allowed to stir for an hour before adding 0.5 mL of aqueous ammonia. The resulting solution was allowed to stir overnight. The still wet material was autoclaved with 10 mL of water at 160°C for 3 days.

Catalysis

A schematic of the catalytic apparatus used is shown below in Figure 16. A 100 mg sample of MnOx catalyst was placed in a glass tube held between glass wool on both sides of the tube. Samples were then heated as a carrier gas (1% O_2 in He) passed through the sample, equilibrating for 1 hour. The carrier gas was then bubbled through isopropanol and passed over the catalyst for 15 minutes. The effluent isopropanol and acetone were finally collected by condensation with liquid nitrogen and analyzed by gas chromatography using a 10 m Carbowax packed column. A typical catalytic run was carried out at 200°C with a flow rate of 10° mL/min.

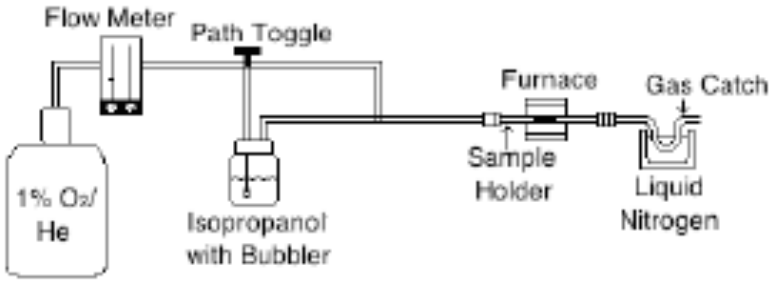

Figure 16. Schematic of catalysis apparatus

Characterization

Scanning electron microscopy (SEM) analysis was carried out with a LEO 435VP scanning electron microscope. A Morgagni Instruments Transmission Electron Microscope was used to capture TEM images. Elemental analysis was done using atomic absorption (AA) spectroscopy using a Varian AA240FS spectrometer. Thermogravimetric analysis (TGA) was performed with a TA Instruments model Q50 TGA. Powder X-ray diffraction (XRD) patterns were recorded with a Rigaku Miniflex diffractometer. Brunauer-Emmett-Teller (BET) surface area measurements were acquired through N_2 adsorption-desorption using a Micromeritics Gemini V Surface Area

Analyzer. Samples were prepared for BET by purging with N_2 at 200 °C using a Micromeritics Flowprep 060 Sample Degas System.

Results and Discussion

Synthesis and Characterization

Allyl and propargyl alcohols were chosen as reducing agents due to their similar polarity as butanol. It was expected that they would partition into the butyric acid emulsion and lead to porous spheres when reacting with permanganate. The added reactivity of having double/triple bonds in addition to the alcohol group is expected to go increase the reaction rate, resulting in more nucleation sites. This in turn should lead to smaller spheres and higher surface areas.

Synthesis of manganese oxides with unsaturated alcohols in the presence of butyric acid and potassium permanganate yielded relatively monodisperse spheres exhibiting hierarchal structure, as seen in Figures 17-19. As seen in the TEM images, the spheres are made up of aggregates of nanoplatelets of about 10 nm in size, similar to the butanol spheres.[22] Spheres made with allyl alcohol (AOHMnOx) had an average diameter size of 156±60 nm, and those made with propargyl alcohol (POHMnOx) had and average diameter size of 143±49 nm. In comparison, the butanol spheres had an average diameter size of 379±15 nm. Thus, syntheses with unsaturated alcohols did produce smaller spheres, as hypothesized. However, smaller spheres were also accompanied by a loss of monodispersity compared to the butanol/permanganate system. The reaction rate was also much faster than in the butanol reaction, turning brown upon mixing. In comparison, the butanol reaction takes over 10 minutes before any precipitate was seen. This supports our hypothesis of faster reaction due to the presence of two reactive sites, and thus smaller nanospheres.

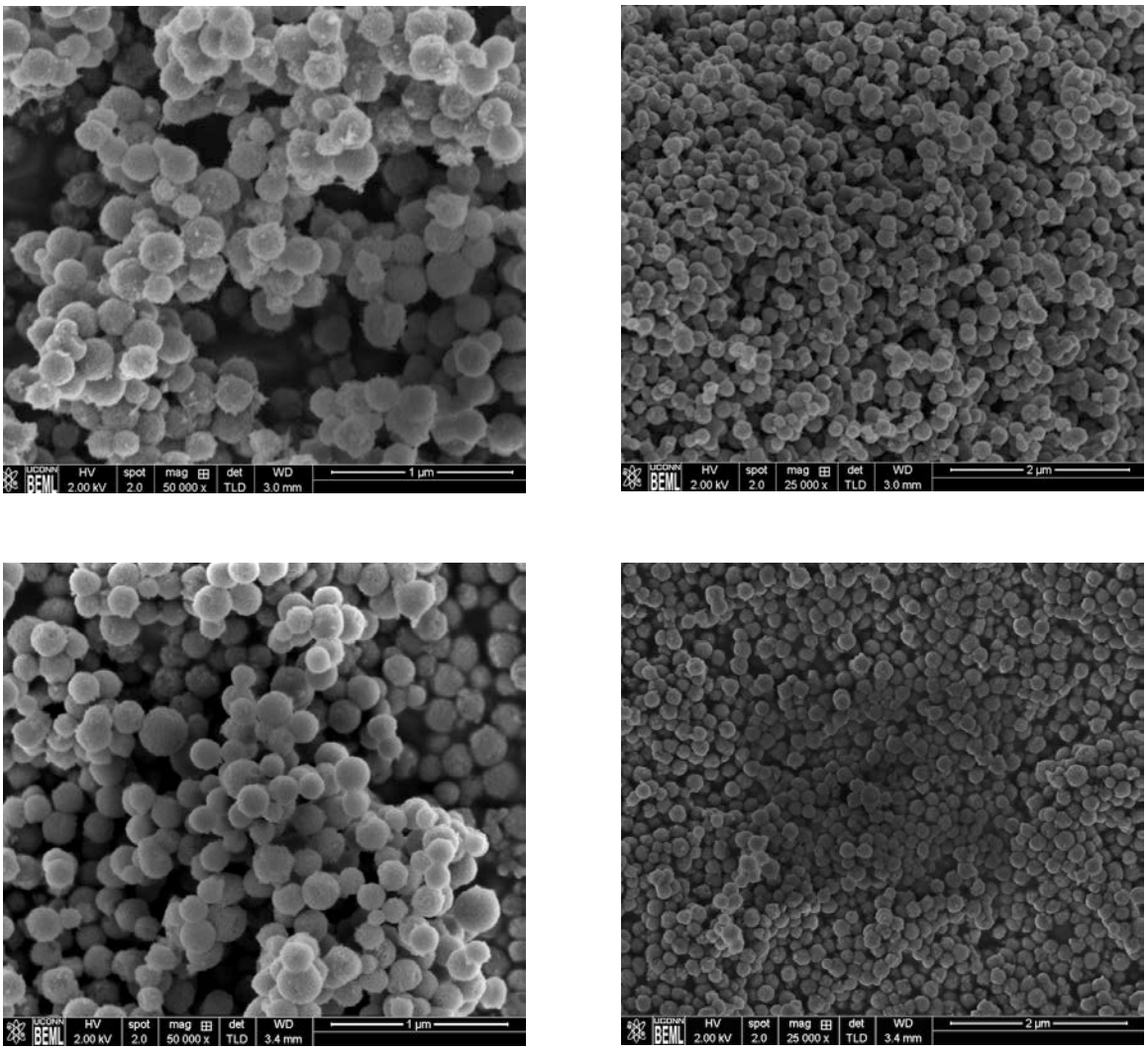

Figure 17. High Res SEM images of, from top to bottom : AllylOH MnOx and PropargylOH MnOx

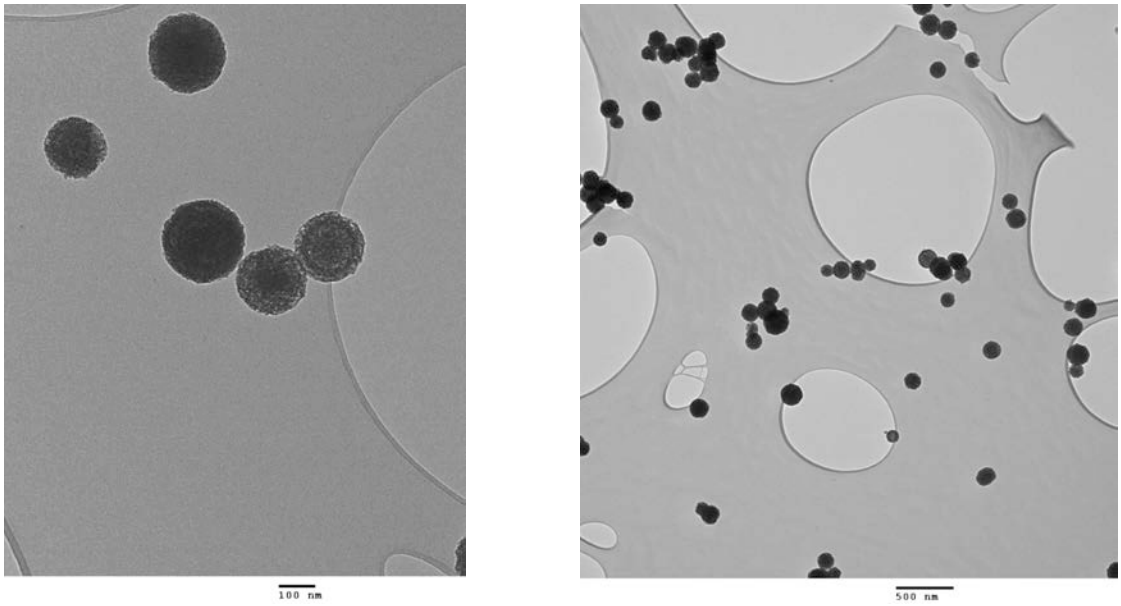

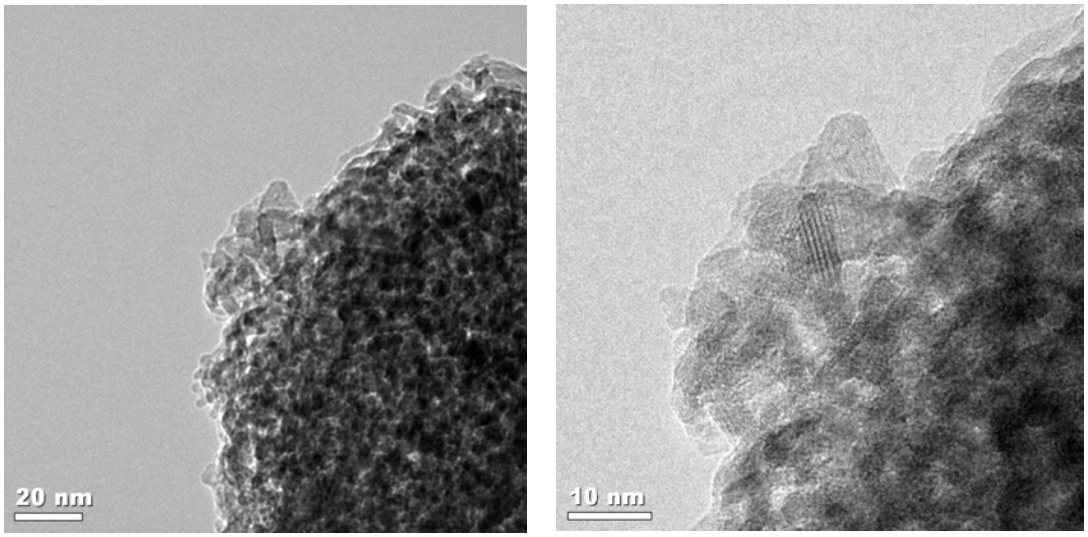

Figure 18. TEM and High Res TEM images of AllyOH MnOx highlighting herarchal structure, tiny platelets aggregating to form proous spheres.

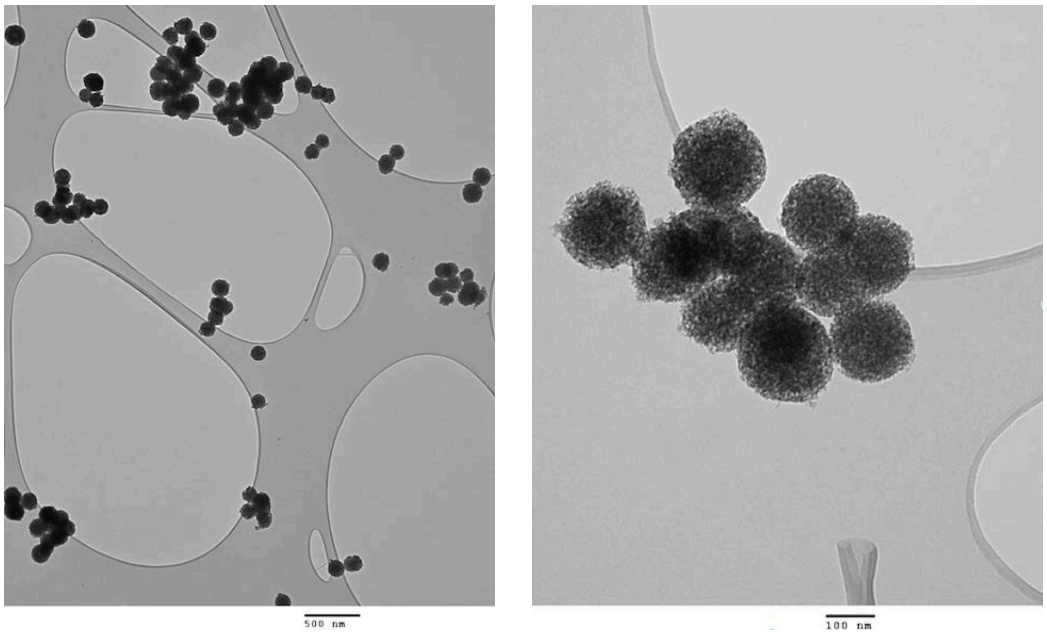

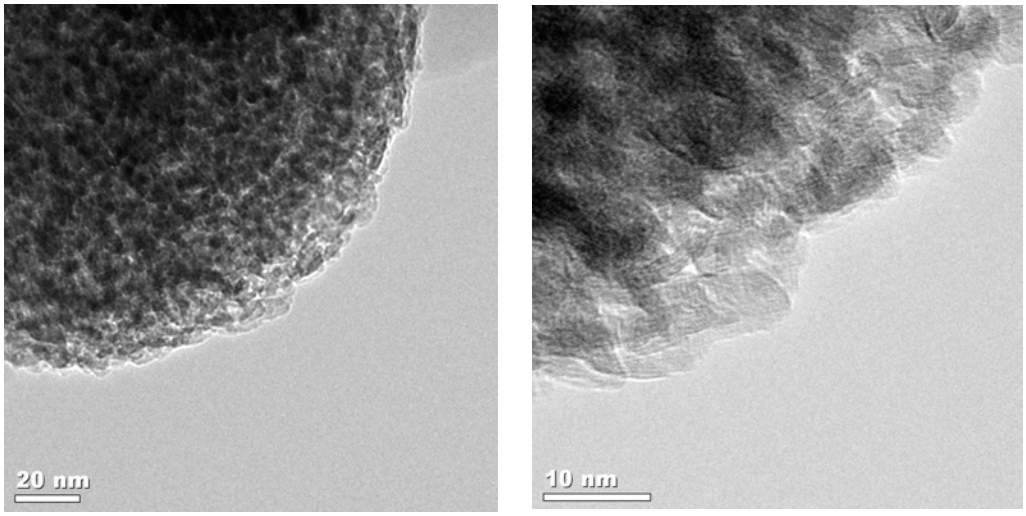

Figure 19. TEM and High Res TEM images of PropargylOH MnOx highlighting herarchal structure, tiny platelets aggregating to form porous spheres.

Elemental analysis showed that the average percentage of manganese was 56.71% in the AOHMnOx and 59.47% for POHMnOx. Residual potassium was also present and made up 0.116% in the AOHMnOx and 0.0598 % in the POHMnOx. Thermogavimetric anaylsis of these spheres are shown below in Figure 20. Slow heating up to 600°C showed that the AOHMnOx were composed of about 12% of water and about 9% in the POHMnOx, as seen by decrease in weight from 25-200°C. Tabel 1 below summarizes these results in comparison to the hollow spheres and butanol spheres. Further weight loss up to 400°C in the AOHMnOx and up to 475°C in the POHMnOx is attributed to the loss of more strongly adsorbed water as well as removal of lattice oxygen as the material begings to decompose . At around 500°C in the POHMnOx a sharp decrease in weight is seen as the material becomes Mn_2O_3. The empirical formula of AOHMnOx, as determined by TGA and AA, was determined to be $K_{0.003}MnO_{1.95} \bullet 0.667H_2O$. The formula of POHMnOx was found to be $K_{0.002}MnO_{1.82} \bullet 0.5H_2O$.

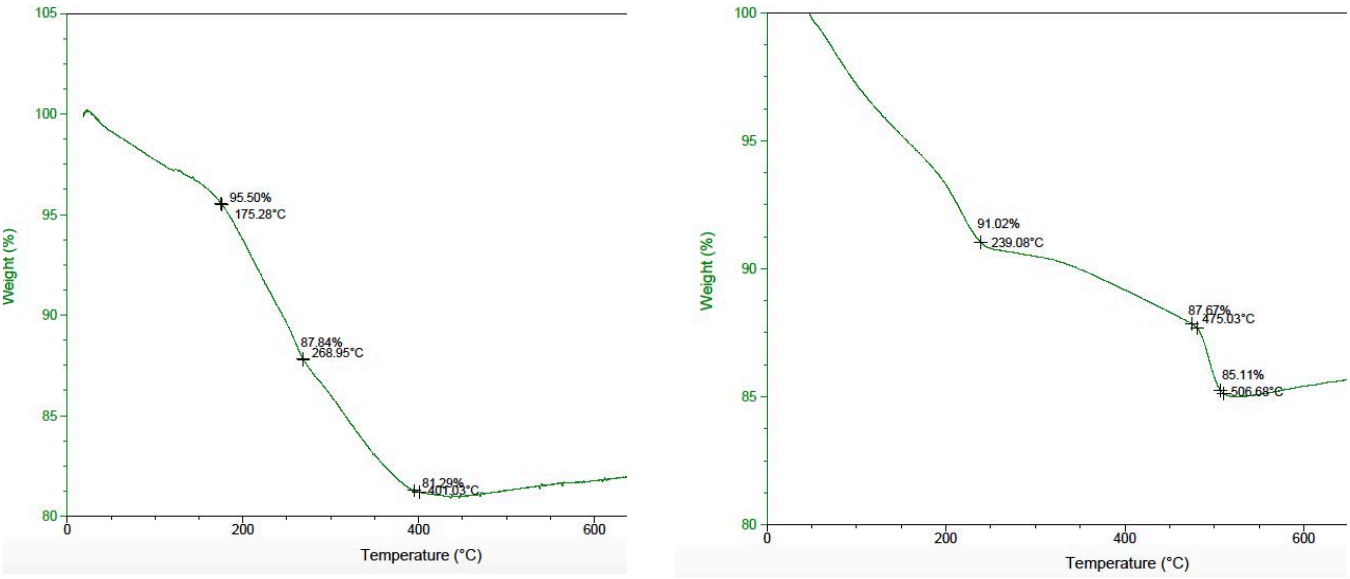

Figure 20. Left to right, TGA graphs of spheres made with allyl alcohol and propargyl alcohol

Average oxidation states were determined through thiosulfate titrations. For propargyl alcohol the average oxidation state was found to be 3.73, and for ally alcohol, 3.49. The values are in agreement with previously reported values. [21,22]

Table 1 Summary of characterization results in comparison to the butanol and hollow spheres

	AOHMnOx	POHMnOx	Butanol Spheres	Hollow Spheres
% Mn	56.71%	59.47%	55.8%	---
% K	0.116%	0.0598 %	0.74%	---
% Water	12%	9%	12%	---
Average Mn Oxidation State	3.49	3.73	3.59	3.83
BET Surface Area	280	260	243	233

X-ray diffraction analysis showed both materials to be amorphous, as seen in Figure 21. Upon closer inspection of the high-resolution TEM images shown previously, Figures 18 and 19, some short-range crystallinity can be seen. However these arrangements are on an extremely small scale and are not prevalent enough to make a crystalline structure, resulting in an amorphous XRD pattern.

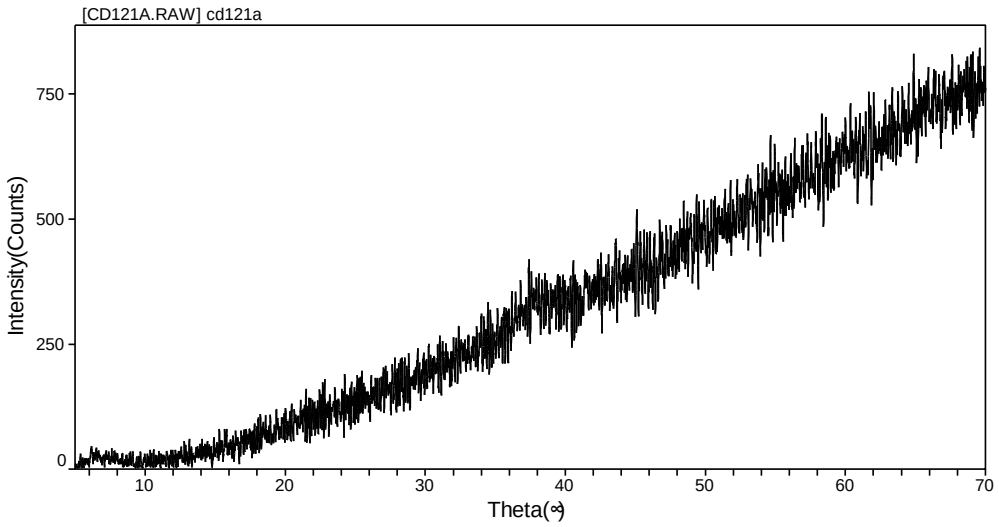

Figure 21. XRD pattern of the AOHMnOx, similar results seen for the POHMnOx

BET surface area analysis showed spheres made with allyl alcohol and propargyl alcohol having an impressive 280 m^2/g and 260 m^2/g, respectively. These surface areas are higher than many other reported high surface area material, including those previously synthesized by the Ching group, shown in Table 1. [22,33] Overall, our hypothesis on the use of unsaturated alcohols is supported. In comparison to the butanol spheres, the reaction did occur faster (on mixing vs. 10 min), produced smaller spheres (156 nm vs. 379 nm), and led to a higher surface area material (280 m^2/g vs. 243 m^2/g).

Material synthesized with the unsaturated alcohols also showed a great deal of monodispersity, as shown in Figure 22. The AOHMnOx had an average diameter of 156 nm with a standard deviation of 61 nm. The POHMnOx spheres proved to be both smaller and more monodisperse, with an average diameter of 143 nm and a standard deviation of 49 nm. Monodisperse materials are desirable as they translate to uniformity in properties. And while other methods are available to form monodisperse spheres, they often require multiple steps, harsh reaction conditions, and longer reaction times of hours or days.[34] In contrast, our spheres are prepared in a one-pot synthesis under ambient conditions in water.

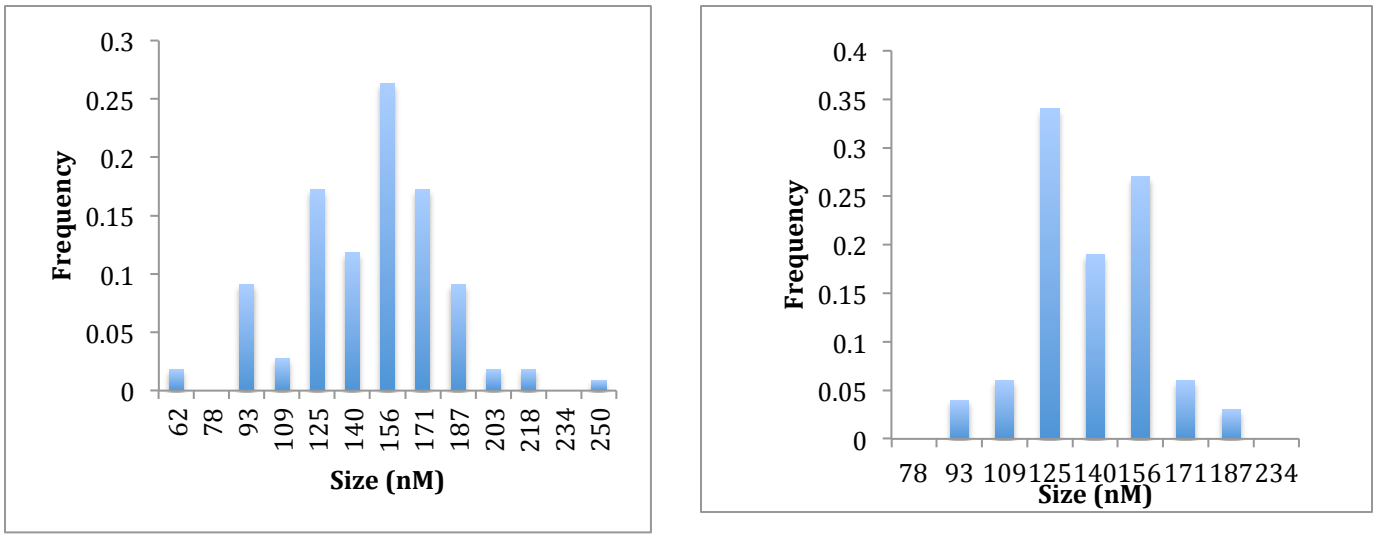

Figure 22. From left to right: Histograms showing frequency of sphere diameters of materials made with allyl alcohol and propargyl alcohol

Dependence on Reaction Conditions

Syntheses of the control spheres were altered by changing the temperature as well as the reaction time. TEM images shown in Figure 23 higlight the results of these experiments. Overall, an increase in temperature led to distortion of morphology while a decrease in temperature had minimal effects. These observation could possibly be due a

disruption of the emulsions as more energy is placed into the sytem through heating. The time alloted for the reaction to occur did not seem to have any effect on the size of the spheres. Comparing images B-F in Figure 23, spheres all roughly had diamteres slighlty larger than 100 nm.

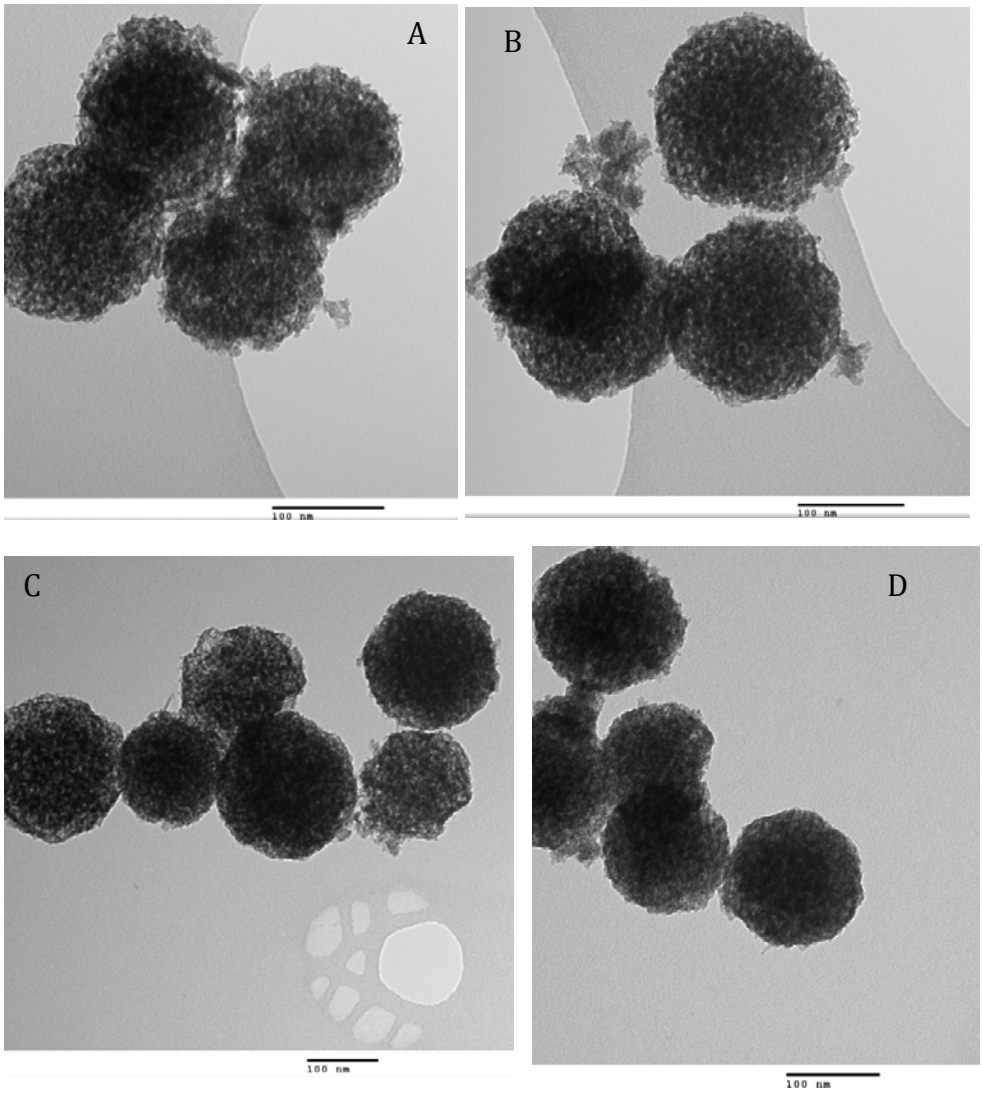

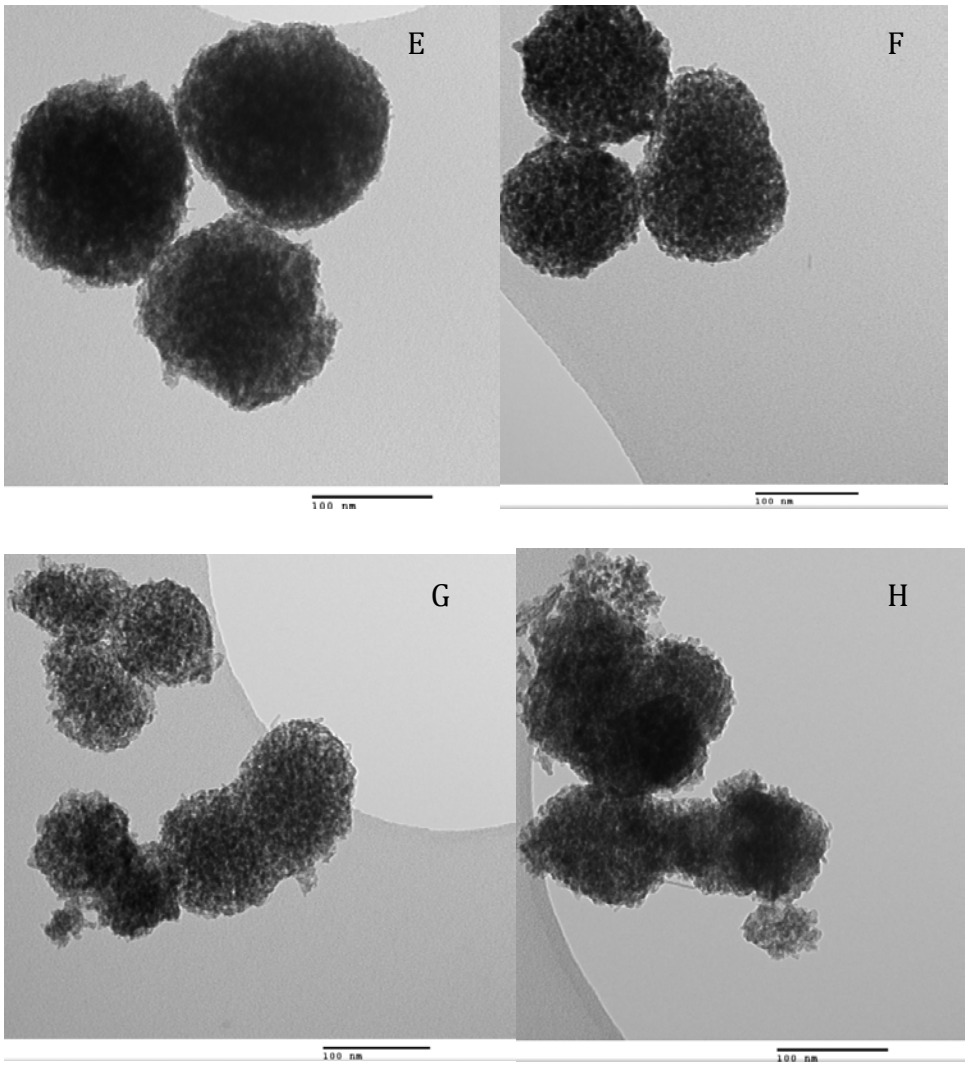

Figure 23. AOHMnOx synthesized at : room temperature for a) 10 min, 5°C for b) 10 min, c) 20 min, d) 30 min , e) 40 min, and f) 60 min. 33°C for g) 5 min and h) 10 min.

Previous research by the Ching group has shown that varying the concentration of $KMnO_4$ in reactions with BuOH leads to changes in particle size, with a direct relationship between particle size and increasing $KMnO_4$ concentration.[22] These findings were tested on the reactions using allyl and propargyl alcohol, by either doubling or halving the $KMnO_4$ concentration. Figures 24 and 25 below outline the results of these experiments. Spheres that were synthesized with twice as much $KMnO_4$ had diameters upwards of 100 nm. Those with only half the concentration had much smaller diameters

of about 60-70 nm. However, when compared to the control spheres, no significant difference is seen between those with twice as much $KMnO_4$ as the control spheres also had diameters upwards of 100 nm.

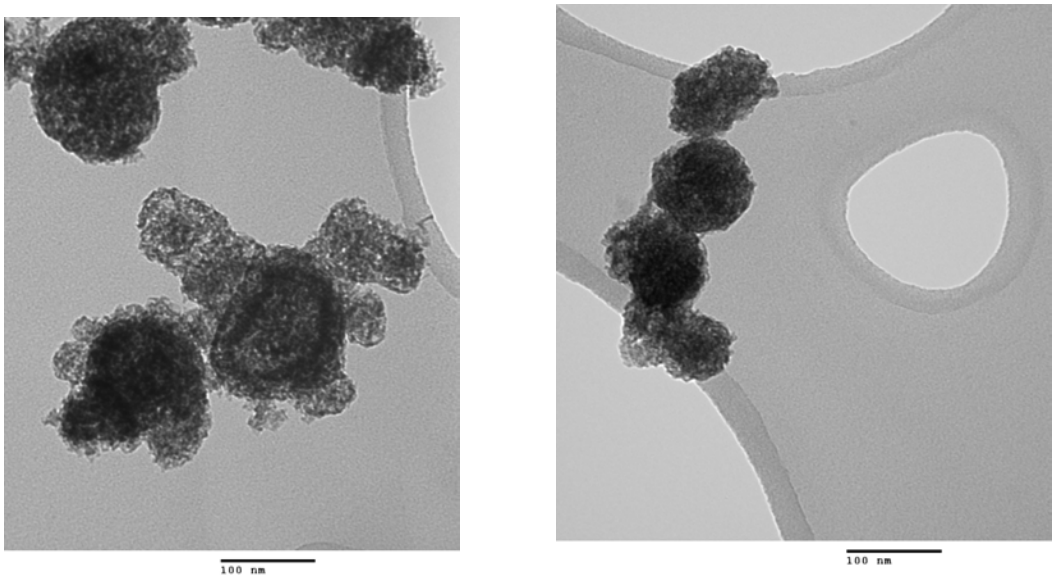

Figure 24. From left to right AOHMnOx with: 2x [$KMnO_4$] and 0.5 [$KMnO_4$]

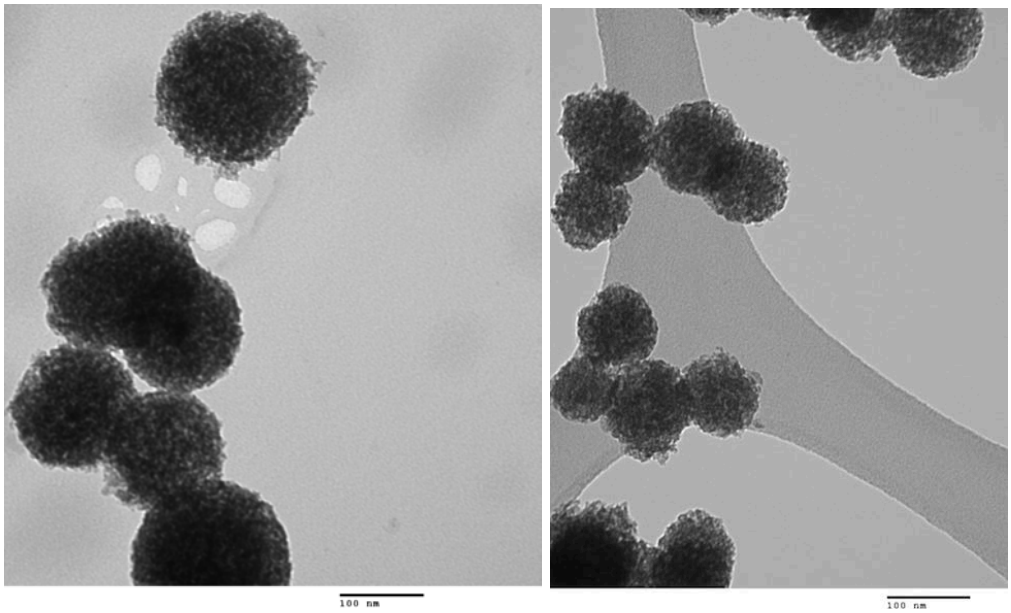

Figure 25. From left to right POHMnOx lwith: 2x [$KMnO_4$] and 0.5 [$KMnO_4$]

Thermal Stability

The effects of calcination on morphology and surface area were also studied. An obvious trend was seen, as the temperature of calcination increased, the surface area decreased. Further there was a noticeable distortion in morphology, especially at 600°C in which there are no longer any distinct spheres and instead low surface area, non-porous materials are seen. These results are consistent with the TGA data shown previously in which, after 400°C, the material begins to decompose to Mn_2O_3. The change in morphology is due to sintering. At higher temperature, the material begins to melt and fuse, resulting in a complete loss of morphology. The extremely low surface areas seen at 600°C are in agreement with other studies.[35,36] These results are summarized in Figures 26 and 27 below.

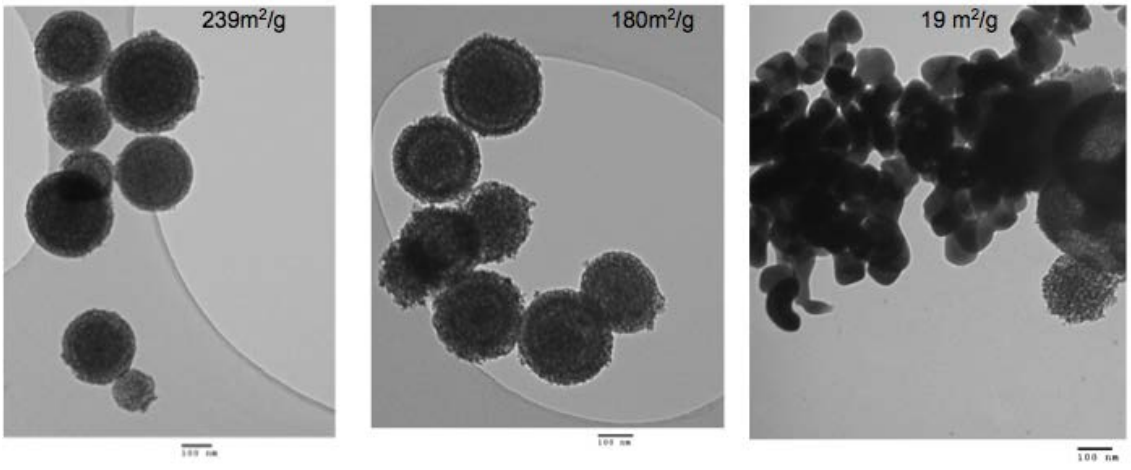

Figure 26. TEM images of AOHMnOx calcined at 200, 400, and 600°C

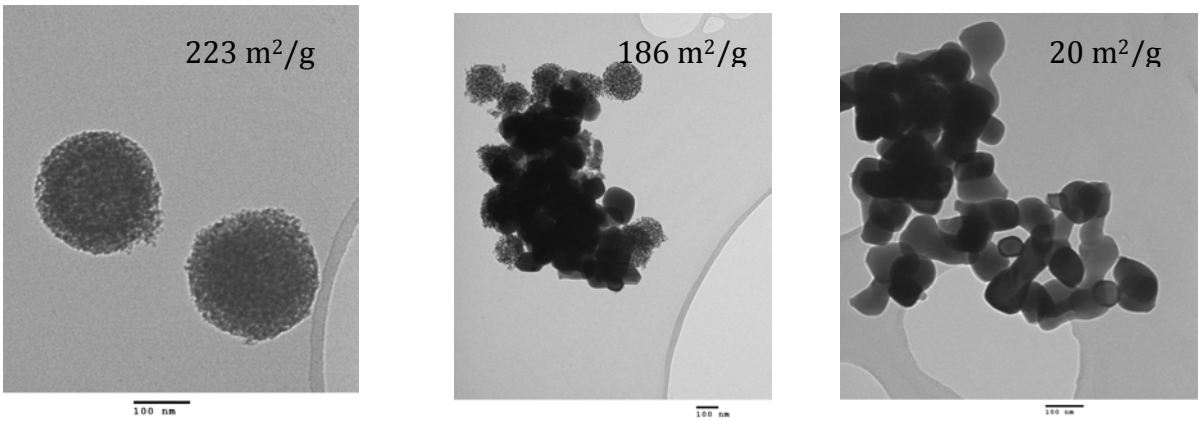

Figure 27. TEM images of POHMnOx calcined at 200, 400, and 600°C

Ethylene Glycol & Glycerol

Manganese oxides made with ethylene glycol or glycerol exhibited a crumpled tissue morphology, similar to that seen in the control reaction, Figure 28. The thought was that ethylene glycol and glycerol would reside in the aqueous phase and result in hollow sphere morphology similar to that observed in reactions between $KMnO_4$ and Mn^{2+}. These materials were generally not monodisperse and were composed of sheets, rather than the platelets seen in the materials made with unsaturated alcohols. Indeed, the morphology is reminiscent of product generated by reacting in the absence of butyric acid.

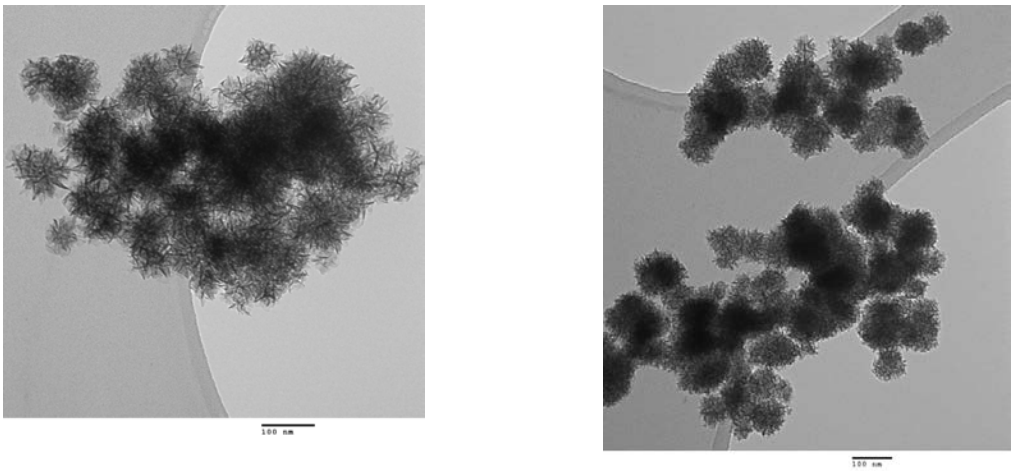

Figure 28. Left to right: TEM image of manganese oxide materials made with ethylene glycol and glycerol.

Catalysis

MnOx are excellent catalysts for the conversion of isopropanol to acetone. A standard catalytic reaction was done at 200°C and a flow rate of 10 mL/min. The AOHMnOx showed a 91% conversion rate of isopropyl alochol to acetone, a high percentage for a relatively low temperature. Other reports of such a high conversion at a low temperature are of spheres that have been doped with a transition metal. [37,38] The POHMnOx had a 78% conversion, signifiacantly lower than the AOHMnOx, but still decent activity. A GC trace of over 90% catlytic conversion with AOHMnOx catalyst is shown below, Figure 29. In general the AOHMnOx materials were on par with both the undoped and doped hollow spheres previously synthesized in the Ching lab at 200°C. At 250 °C, however, the doped hollow spheres have a higher conversion rate (up to 98% in Cu doped spheres) compared to AOHMnOx and POHMnOx. The undoped hollow spheres at 250°C have conversions that are slightly lower than then AOHMnOx and POHMnOx. AOHMnOx proved to be better catalysts than the butanol spheres, which at max showed about 84% conversion at 200°C. [22] Table 2 summarizes these findings.

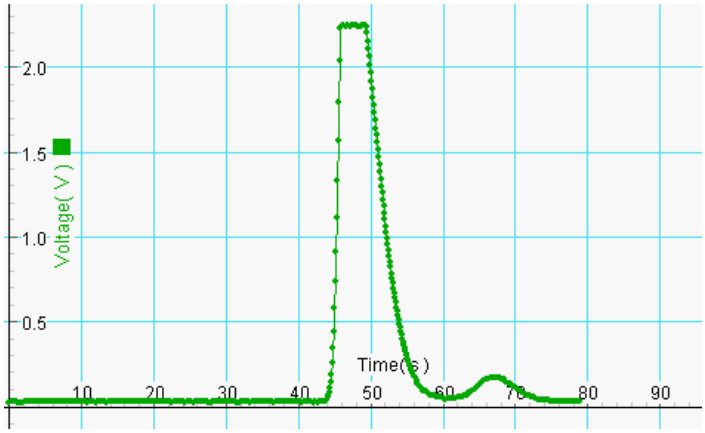

Figure 29. GC trace showing over 90% conversion. Fist peak is acetone, second is isopropyl alcohol.

Table 2: Comparison of Catalytic activity of materials previously synthesized

Material	Catalytic Activity at 200°C (%)	Catalytic Activity at 250°C (%)
AOHMnOx	91	94
POHMnOx	78	94
Butanol Spheres	84	---
Cu Doped Hollow Spheres	92	98
Iron Doped Hollow Spheres	96	94
Undoped Hollow Spheres	92	89

The catalytic activity of materials made with unsaturated alcohols was studied under varying conditions. Firstly, the effects of temperature on catalytic activity were studied. It was found that as the temperature increased, so did the catalytic activity, which was expected.[39, 40] Table 3 summarizes these findings.

Table 3: Catalytic conversion percentages of materials made with ally alcohol and propargyl alcohol at various temperatures.

AllylOH		PropargylOH	
Temperature °C	Catalysis %	Temperature °C	Catalysis %
150	85.03	150	76.3
200	91.04	200	77.59
250	94.16	250	93.94

Next, the effects of the gas flow rate on catalytic activity of were studied. A general trend was seen in which an increase in flow rate led to a decrease in catalytic activity. These results are likely due to isopropyl alcohol passing through the catalyst too quickly and not having enough time to adsorb onto the catalyst. Results are summarized in in Table 4, below.

Table 4: Catalytic conversion percentages of AOHMnOx materials at various flow rates.

Flow Rate mL/min	Catalysis %
10	87
20	84
30	69
40	56

Lastly, the effects of time-on-stream were studied. A general trend was seen in which as the time on stream was increased, catalytic activity decreased, as seen in Table 5. This observation was attributed to the catalyst instability with time when exposed to the reactants. This is supported by TEM images shown in Figure 30, which shows the morphological changes undergone by the catalyst. A decrease in catalytic activity is attributed to a loss of surface area as the porous spheres of aggregated nanoplatelets breaks up into individual nanospheres that are larger than the original nanoplatelets. This in turn leads to a decrease in active sites for the catalyst as the time on stream in increased, and therefore catalytic activity is reduced. Table 6 portrays this loss of surface area.

Table 5: Catalytic conversion of AOHMnOx material as time on stream increases, 10 min is the control reaction

Collection Time (min)	Catalysis %
10	87
60	71
180	62

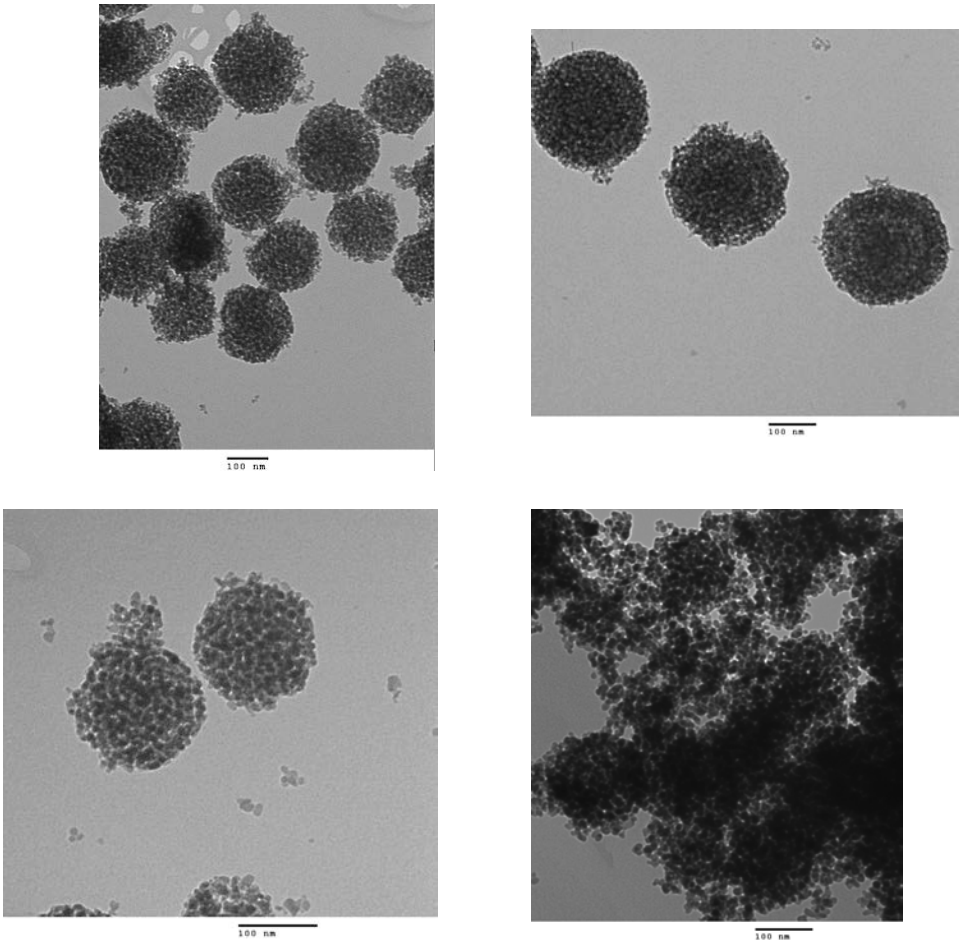

Figure 30. TEM images of AOHMnOx from top, left to right: after 10 min, 1 hour Bottom, left to right 2 hours, and 3 hours time on stream.

Table 6: Loss of AOHMnOx surface area as time on stream increases

Time on Stream (Min)	BET m^2/g
10	114
60	62
180	49

Doping

Transition metal doping has been shown to increase catalytic activity (Cu) as well as increasing surface area (Fe). So, materials synthesized using allyl alcohol and propargyl alcohol were isomorphously doped with copper and iron. Spheres were synthesized with a 0.2:1 ratio of Cu:Mn and a 0.15:1 ratio of Fe:M.. The average ratio of metal: manganese that was actually incorporated into the material was then determined by atomic absorption spectroscopy and results are shown in Table 7. Copper was poorly incorporated into the materials, consistent with data previously obtained in our research group.[41] Iron was almost completely incorporated into both of the materials, again in agreement with previous results. [41] It is believed that since iron has relatively the same size as manganese, as well also sharing similar oxidation states, it easy for iron to isomorphously substitute for manganese.

Table 7: Average Metal:Mn ratio that was incorporated into the material

Metal: Mn	AllyOH	PropargylOH
Cu:Mn	0.03:1	0.015:1
Fe:Mn	0.13:1	0.14:1

Overall, copper doping seemed to have no effect on the morphology of materials

made with allyl alcohol and caused some distortion of morphology for materials made with propargyl alcohol, though platelet morphology was still evident. Iron doping, however caused morphological changes in both materials, resulting in hollow or yolk-shell structures, Figure 31. This yolk-shell structure has been seen before with iron-doped materials. Though it is not clear what causes this structure one possible explanation for this may be the formation of a magnetic core with a manganese oxide shell.[42]

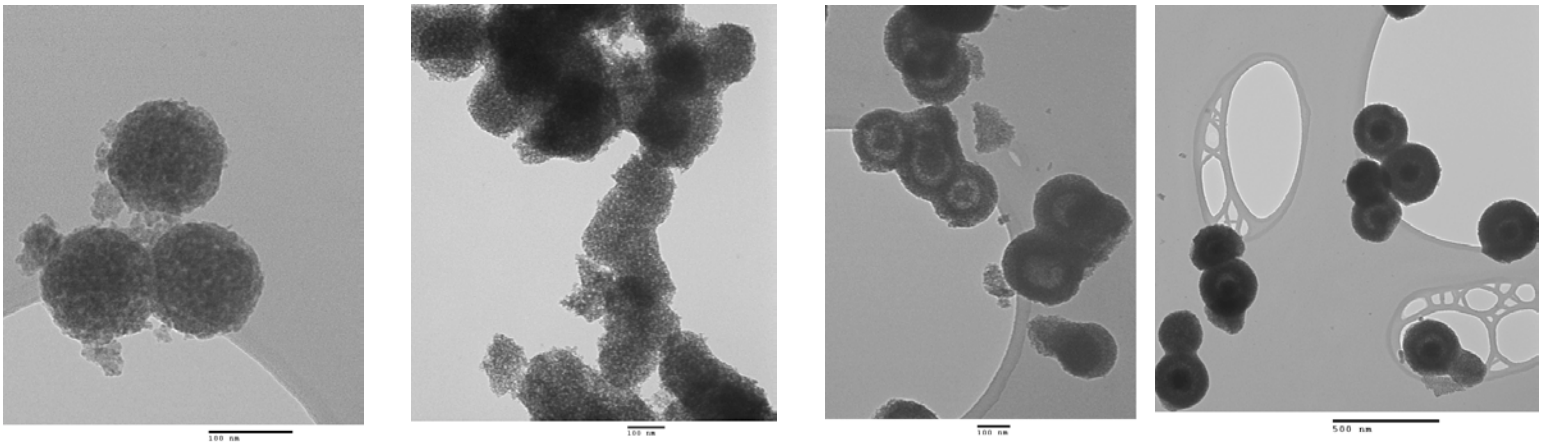

Figure 31. Left to right: Morphological effects of copper doping on allyl alcohol materials and propargyl alcohol materials, morphological effects of iron doping on allyl alcohol materials and propargyl alcohol materials.

MnOx materials were also doped via insipient wetness impregnation with alkali metal acetates. These procedures were carried out to examine if alkali metal cations can be dispersed into the pores and then heat treated to yield crystalline phases such as spinel, birnessite, and hollandite that still have porous morphologies with high surface areas. Materials were doped with Li, K, or Na cations by mixing solutions of the cation salts with MnOx, then allowing the resulting slurry to dry with the salts impregnated into the porous MnOx. After doping, materials were calcined at 450°C with the hopes of inducing

crystalline structure. Separately, K doped materials were also calcined at 600 °C. Pervious research has shown lithium being able to induce spinel structures [43] and potassium inducing cryptomelane structures, a naturally occurring tunneled manganese oxide with potassium in the tunnel sites.

For lithium, synthesis reactions were done in a 0.25:1 and 0.5:1 ratio of Li:Mn, resulting in similar XRD patterns corresponding to spinel manganese oxide. A representative XRD pattern is shown below in Figure 32. Indexing of the patterns with entries in the Powder Diffraction Files (PDF) database revealed possible spinel structures that included: $Li_{1.27}Mn_{1.7304}O_4$, $LiMn_2O_{4,}$ $Li_4Mn_5O_{12}$ (PDF#s 51-1582, 35-0787, and 46-0810, respectively). TEM analysis confirmed the presence of a crystalline structure with long rods, as opposed to porous spheres seen in the original amorphous material, Figure 33. In this case there was a loss of morphology as well as porosity.

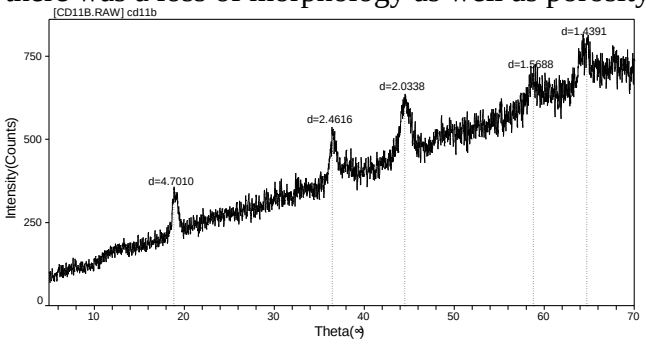

Figure 32. XRD pattern of Li doped ally alcohol material through impregnation

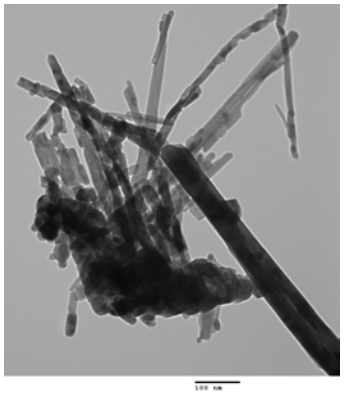

Figure 33. TEM Image crystalline manganese oxide, spinel structure.

For potassium doped materials, calcination at 450 °C was performed after doping reactions with 0.5:1 and 1:1 ratios of K:Mn. No significant difference was observed between products from the two doping ratios, when analyzed by XRD. A representative XRD pattern is shown below in Figure 34. A possible structure was found to be $K_2Mn_4O_8$ (PDF #16-0205) corresponding to the birnesite structure. And while no real difference in pattern was seen through XRD analysis, TEM images, Figure 35, show some morphological differences. The 0.5:1 material showed long rods similar to those of the spinel structure while the 1:1 material showed an abnormal, indistinctive morphology.

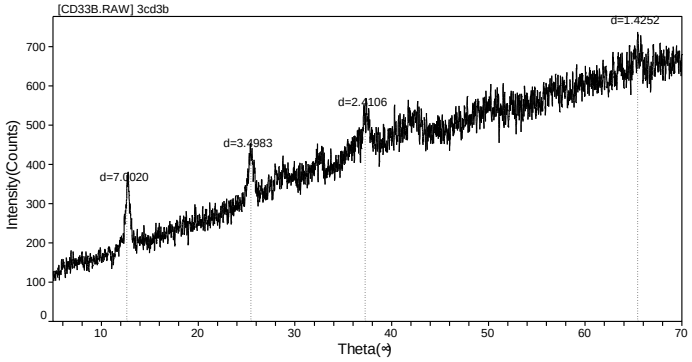

Figure 34. XRD pattern of K doped ally alcohol material through impregnation

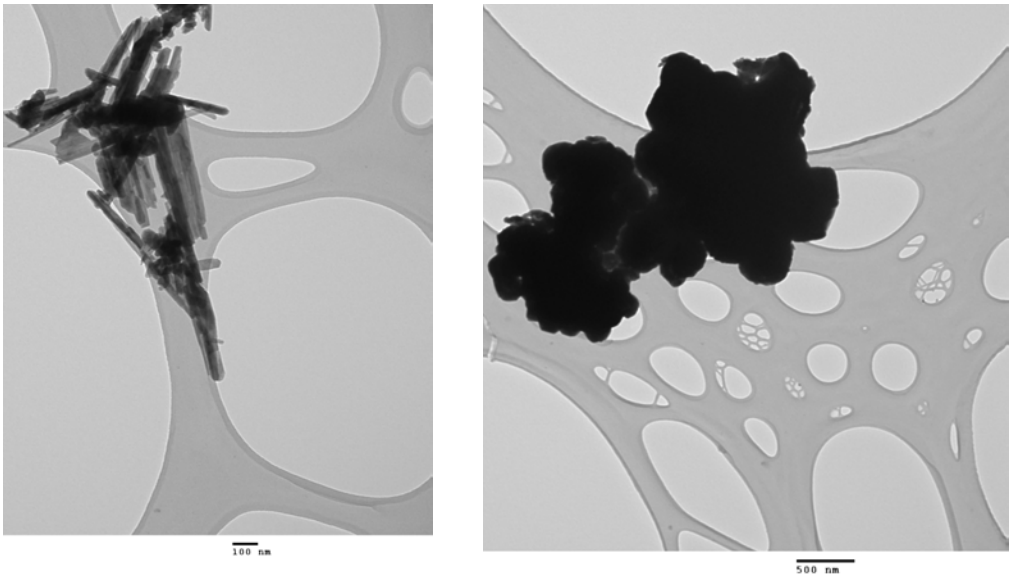

Figure 35. Left to right TEM image of 0.5:1 and 1:1 K doped material.

For potassium, calcined at 600 °C, doping reactions were done in a 0.5:1 and 1:1 ratio of K:Mn. With the 0.5:1 doped materials, XRD patterns were similar to those from material calcined at 450°C. The 1:1 doped material however showed an XRD pattern representative of cryptomelane (PDF#42-1348), Figure 36. TEM images, Figure 37, show a distorted morphology, once again probably due to sintering of the materials at high temperatures.

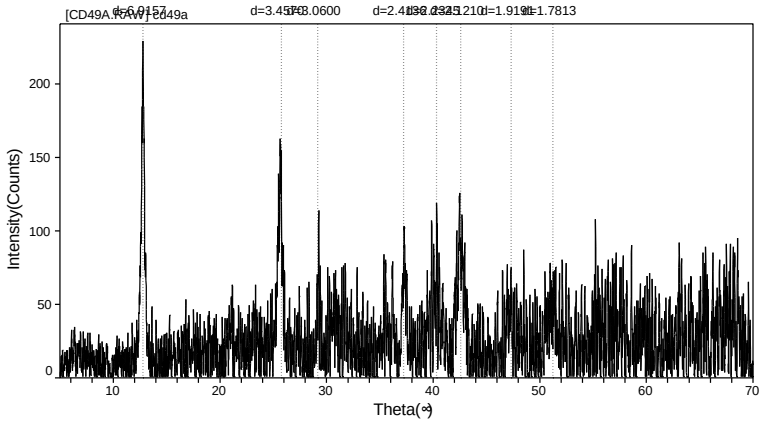

Figure 36. XRD pattern of K doped ally alcohol material through impregnation, calcined at 600°C

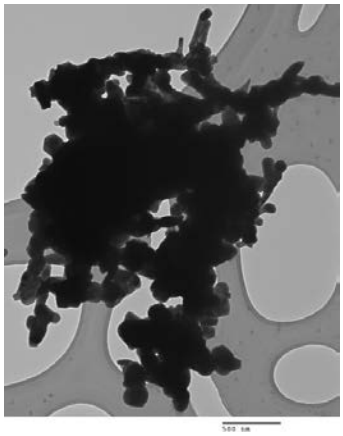

Figure 37. TEM of K doped ally alcohol material through impregnation, calcined at 600°C

In regards to sodium, doping reactions were done in a 0.5:1 and 1:1 ratio of Na:Mn, with no significant difference was observed when analyzed by XRD. A

representative XRD pattern is shown below in Figure 38. The possible structure, as determined by indexing to PDF #27-0752, was $Na_{0.7}MnO_2$. This structure was determined to be a dehydrated version of birnessite, which has been previously synthesized through sol-gel methods.[25] While XRD showed similar patterns for both 0.5:1 and the 1:1 doped materials, the 1:1 doped materials exhibited a unique "starburst" or "solar flare" morphology that has not been seen in materials doped with lithium or potassium. While the starburst morphology was not the dominant morphology, it was prevalent enough to be considered significant. TEM images below, Figure 39, compare the more common morphology of clumped rods against the starburst morphology seen. Calcination experiments of the 1:1 Na:Mn was repeated, this time having the materials calcined for 6 hours, in contrast to the standard 2 hours, in hopes of yielding the starburst morphology as the most prominent. However, the XRD pattern was relatively the same as the materials calcined for 2 hours. TEM analysis also did not show any increase in the starburst morphology.

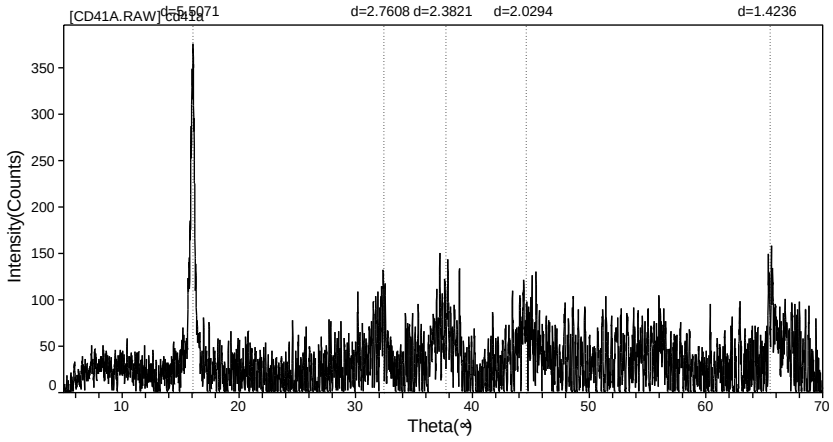

Figure 38. XRD pattern of Na doped ally alcohol material through impregnation

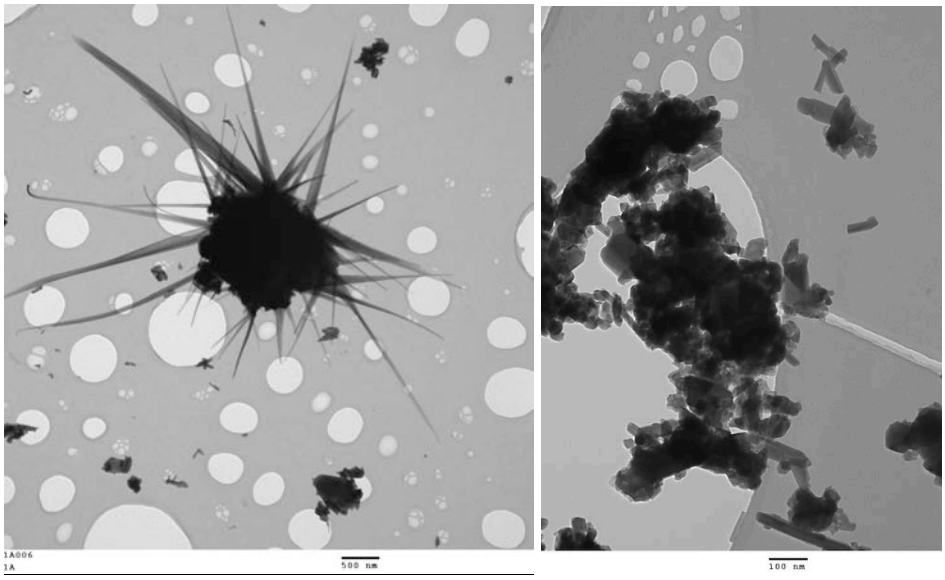

Figure 39. TEM of Na doped ally alcohol material through impregnation, showcasing the different mopholgies seen. Left: starburst, Right: clumped rods

Hydrothermal Treatment

Hydrothermal treatment of AOHMnOx that had been doped with magnesium through insipient wetness methods yielded Manganite of formula MnO(OH) as determined by XRD, shown in Figure 40. Analysis by TEM showed a common “tooth” morphology, in which the bottom of the crystals were rounded out and grew to a point, as seen in Figure 41. Interestingly, when the material was allowed to dry before being hydrothermally treated, Huasmannite (PDF# 24-0734) was obtained, as seen in the XRD pattern in Figure 42. These materials had a rod shaped morphology, which still had some porous aggregates on top of them, Figure 43.

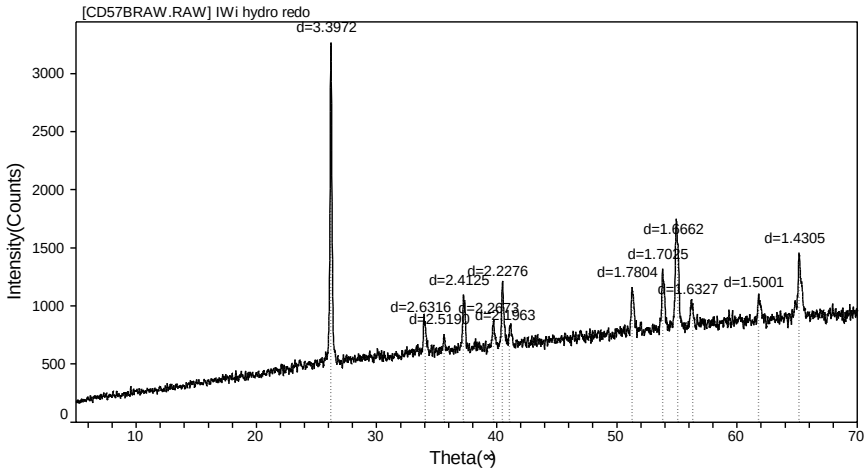

Figure 40. XRD pattern of Mg doped ally alcohol material through impregnation, followed by hydrothermal treatment.

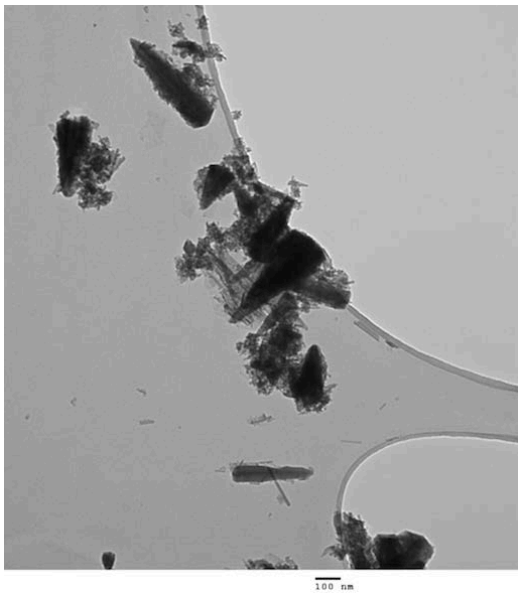

Figure 41. TEM image of Mg doped ally alcohol material through impregnation, followed by hydrothermal treatment showcasing a tooth-like morphology

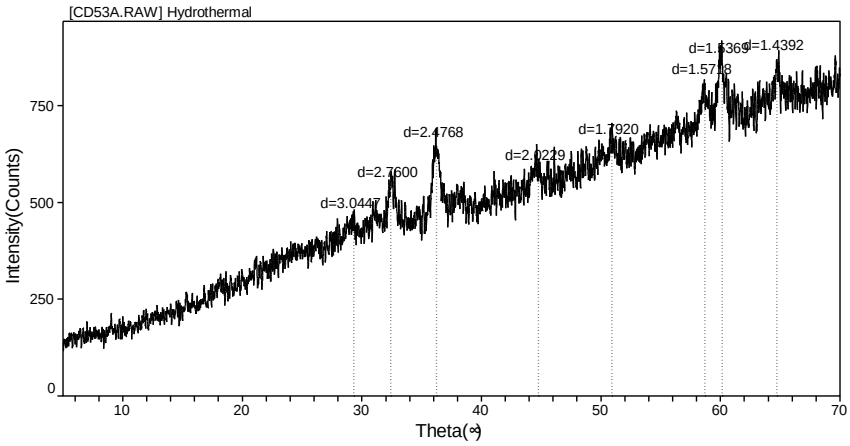

Figure 42. XRD pattern showcasing haumannite after hydrothermal treatment of insipient wetness Mg doped ally alcohol materials, that were dried beforehand

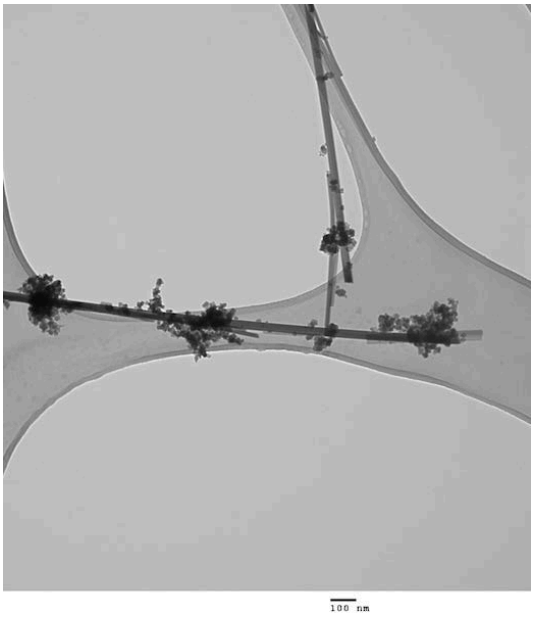

Figure 43. TEM image of Mg doped ally alcohol materials after hydrothermal treatment, that were dried beforehand

AOHMnOX materials were also doped isomorphously with Mg, followed by hydrothermal treatment. The XRD pattern is shown below in Figure 44. The possible structure, as determined by indexing to PDF #24-0736 and 17-0510 were $MgMnO_3$ and Nsuite ($Mn(O,OH)_2$, respectively. These materials formed large “twin crystal”

morphologies, with rods having a wide variety of thicknesses. Diameters ranged from a nanometer scale to over 2 microns wide, Figure 45.

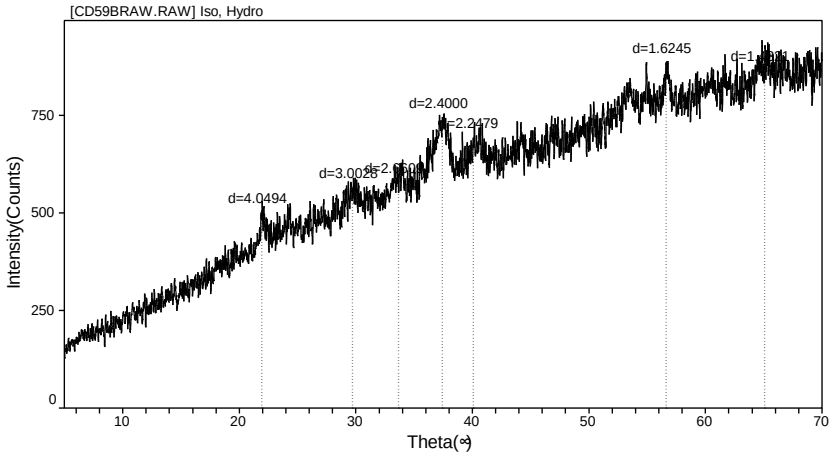

Figure 44. XRD pattern of isomoprpohus Mg doped ally alcohol material, followed by hydrothermal treatment.

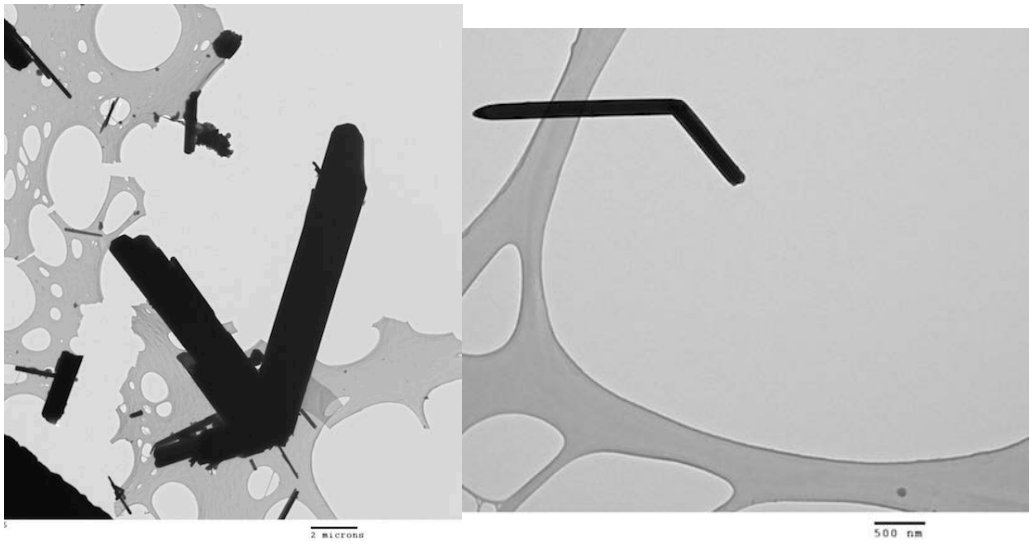

Figure 45. TEM image of isomoprpohus Mg doped ally alcohol material, followed by hydrothermal treatment. Left image has a twin-crystal with a diameter of over two microns, right dimaeter is about 150 nm.

Conclusion

In summary, we have been able to successfully synthesize porous manganese oxides using unsaturated alcohols as the reducing agent in a reaction with $KMnO_4$, in the presence of butyric acid. These materials have shown a good deal of monodispersity, though not as impressive the spheres made with butanol. However, the reaction proceeds at a much quicker rate (instant vs. 10 min), materials were over twice as small (156 vs 379 nm) and had a larger surface area (280 m^2/g vs. 243 m^2/g). These results supported our hypothesis of more reactive sites leading to a faster reaction, smaller particle size, and higher surface materials. Further, these materials have proven to be active catalysts in the conversion of isopropyl alcohol to acetone with about 90% conversion at 200°C for the AOHMnOX and over 90% for both the AOHMnOX and POHMnOX.

Further, we have shown that crystalline structure can be induced through doping with metals followed by heat treatment (calcination or hydrothermal). Doping with Li, K, and Na followed by calcination led to spinel, cryptomelane, and birnessite structures, respectively. Doping with Mg, through impregnation, followed by hydrothermal treatment led to the formation of either Hausmanite or Manganite, depending on whether the product was allowed to dry before hand or not. Isomorphous doping of Mg followed by hydrothermal treatment led to the formation of Nsuite.

Future Work

Further research is needed on the effects of Mg doping on catalytic activity. Magnesium has been shown to stabilize catalyst and can help with the stability of the catalyst as time on stream increases. Further, the catalytic scope of these materials can be expanded by testing the efficiency of these materials in other catalytic reactions such as the conversion of carbon monoxide to carbon dioxide.

Additional work should also be done on the induction of crystalline structure through metal doping followed by heat treatment. The hope of Mg doping followed by hydrothermal treatment was for a result of todorokite, which did not happen. Todorokite is difficult to synthesize by heat treatment due to its large 3x3 interstitial space and so more studies should be done in order to successfully yield this product.

References

1. Post, J. E. *Proc.Natl.Acad.Sci* **1999**, 96,3447-3454.
2. Achurra, E; Lacassie, J.P.; Le Roux, J.P.; Marquardt, C.; Belmar, M; Ruiz-del-Solar, J.;Ishman, S.E., *Sedi. Geo*. **2009**, 217, 128-139.
3. Abramowski, T.; Stoyanova, V., *SGEM*, **2012,** 1, 515-522
4. Chen, C. C.; Golden, D. C.; Dixon,J. B. *Clays Clay Miner*, **1986**, 34, 565.
5. Chen, X.; Li,X.; Jiang,Y.; Shi,C.; Li, X., *Solid State Comm.* **2005**, 136, 94-96.
6. Yousefi,T; Davarkhah,R; Golikand, A.N.; Mashhadizadeh, M.H., *Mater. Sci. Semi. Proc.*, **2013**, 16, 868-876.
7. Suib, S.L., *J.Mater.Chem,* **2008**, 18, 1623.
8. Wei,W.; Cui,X.; Chen,W.; Ivey, D.G., *Chem. Soc. Rev*., **2011**, 40, 1697.
9. Guo,Y.; Guo, H.; Wang, Y; Liu, L.; Chen, W., *RCS Adv.*, **2014**, 4, 14048.
10. Jenness, G.R.; Schmidt, J.R, *ACS Catal.*, **2013**, 3 (12), 2881–2890
11. Degirmenbasi, N.; Coskun, S.; Boz, N.; Kalyon, D. M. *Fuel* **2015**, 153, 620-627.
12. Israel, M.O., *J. Nutr. Food. Sci*., **2015**, S11: S11-001.
13. Hsu, N; Diosady, L.L; Graydon, W.F.;Rubin, L.J., *J. Amer. Oil. Chem. Soc.* **1986**, 63, 1036-1042.
14. Turner, A.; Price, S., *Environ Sci Technol*. **2008**, 42(24),9443-9448.
15. Bagey, S.T.; Gratz, L.D,;Johnson, J.H.;McDonald, J.F, *Environ. Sci. Technol*., **1998**, 32 (9), 1183–1191.
16. Son, YC. ; Makwana, V. D.; Howell, A. R.; Suib, S. L., *Angew. Chem. Int. Ed*., **2001**, 40, 4280–4283.

17. Jing, H.; Keqiang, S.; Daiping,H.; Boqing,X., *Chin J Catal*, **2007**, 28(12),1025–1027.

18. Li, J.; Wang, R.; Hao, J., *J. Phys. Chem. C*, **2010**, 114, 10544–10550.

19. Chen, CU.; Njagi, E.C.; Sun, SP.; Genuino,H.; Hu,B.; Suib,S.L, *Chem. Mater*., **2010**, 22(11), 3313–3315.

20. Kramer, M.; Schimdt, T.; Stowe, K.; Maier, W.F., *Appl. Cata. Gen.* **2006,** 302,257–263.

21. Ching, S.; Kriz, D.A.; Luthy, K.M.; Njagi, E.C; Suib,S.L.,*Chem. Commun*., **2011**, 47, 8286–8288.

22. Ching, S.; Richter, I. J.; Tutunjian, K.A.; Kriz, D.A.; Kovic,Y., *Chem. Commun*., **2015**, 51, 1961.

23. Wang, F.; Dai, H.; Deng, J.; Bai, G.; Ji, K.; Liu, Y., *Environ. Sci. Technol*., **2012**, 46(7), 4034–4041.

24. Hou, J.; Liu, L.; Li, Y.; Mao, M.; Lv, H.; Zhao, X., *Environ. Sci. Technol*., **2013**, 47(23),13730–13736.

25. Ching, S.; Petrovay, D.J.; Jorgensen, M.L.; Suib,S.L., *Inorg. Chem*. **1997**, 36, 883-890.

26. Ching, S.; Welch, E.J.; Hughes, S.M.; Bahadoor, A.B.F.; Suib,S.L, *Chem. Mater*. **2002**, 14, 1292-1299.

27. Kai, K.; Yoshida, Y.; Kageyama, H.; Saito, G.; Ishigaki, T.; Furukawa, Y.; Kawamata, J., *J. Am. Chem. Soc*., **2008**, 130(47), 15938–15943.

28. Chen, H.; He, J.; Zhang, C.; He, H., *J. Phys. Chem. C*, **2007**, 111(49), 18033–18038.

29. Yu, X.; He, J.; Wang, D.; Hu, Y.; Tian, H.; He, Z., *J. Phys. Chem. C,* **2012**, 116(1), 851–860.

30. Xu, M.; Kong, L.; Zhou, W.; Li, H., *J. Phys. Chem. C,* **2007**, 111, 19141-19147.

31. Zeng, H.C, *Curr. Nanosci.*, **2007**, 3, 177-181.

32. Bagai, R.; Christou, G., *Chem. Soc. Rev.*, **2009**, 38, 1011–1026.

33. Mathew,V.; Lim, J.; Kang, J.; Gim, J.; Rai, A.K.; Kim, J., *Electro. Commun.* **2011**, 13, 730-733.

34. Schladt,T.D.; Graf, T.; Tremel, W., *Chem. Mater.*, **2009**, 21(14), 3183–3190.

35. Augustin, M.; Fenske, D.; Bardenhagen, I.; Westphal, A.; Knipper, M.; Plaggernborg, T.; Kolny-Olesiak, J.; Parisi, J., *Beilstein J. Nanotechnol*. **2015**, 6, 47–59.

36. Tang, W.; Wu, X.; Li, D.; Wang, Z.; Liu, G.; Liu, H.; Chen, Y., *J. Mater. Chem. A,* **2014**, 2, 2544-2554.

37. Liu, R.; Yang, Z.Q., *Huan Jing Ke Xue*. **2012**, 33(6),1964-70.

38. Cai, L.; Hu, Z.; Branton, P.; Li, W., *Chi. J. Cata.*, **2014**, 35, 159-167.

39. Akhtar, K.; Khalid, N.; Ali, M., *J.Chem.Soc.Pak.*, **2012,** 34, 263-268.

40. Sriskandakumar, T.; Opembe, N; Chen, CH.; Morey, A.; King'ondu, C.; Suib, S. L., J. *Phys. Chem. A,* **2009**, 113, 1523–1530.

41. Carmichael, J, *Conn. Coll*., **2014**.

42. Estrader, M.; López-Ortega, A.; Estradé, S.; Golosovsky, I. V.; Salazar-Alvarez,G. ; Vasilakaki, M.;. Trohidou, K. N; Varela, M.; Stanley,D.C,; Sinko, M.; Pechan, M.J.; Keavney,D.J.; Peiró, F.; Suriñach,S.; Baró, M.D.; Nogués, J. *Nat Commun.* **2013**, 4, 2960.

43. Yonemura, M.; Yamada, A.; Kobayashi, H.; Tabuchi, M.; Kamiyama, T.; Kawamoto, Y.; Kanno, R., J. *Mater. Chem*., **2004**, 14, 1948–1958.